Molecular Therapy
Original Article

Promoter Methylation-Regulated miR-145-5p Inhibits Laryngeal Squamous Cell Carcinoma Progression by Targeting *FSCN1*

Wei Gao,[1,2,3,4,14] Chunming Zhang,[1,2,3,4,14] Wenqi Li,[1,2,3,4,14] Huizheng Li,[5,14] Jiangwei Sang,[1,2,3,4,14] Qinli Zhao,[1,2,3,4] Yunfeng Bo,[6] Hongjie Luo,[1,2,3,4] Xiwang Zheng,[1,2,3,4] Yan Lu,[7] Yong Shi,[1,2,3,4] Dongli Yang,[1,2,3,4] Ruiping Zhang,[4,8] Zhenyu Li,[4,9] Jiajia Cui,[1,2,3,4] Yuliang Zhang,[1,2,3,4] Min Niu,[1,2,3,4] Jun Li,[1,2,3,4] Zhongqiang Wu,[1,2,3,4] Huina Guo,[1,2,3,4] Caixia Xiang,[1,2,3,4] Juan Wang,[1,2,3,4] Juan Hou,[1,2,3,4] Lu Zhang,[1,2,3,4] Rick F. Thorne,[10,11] Yongping Cui,[12,13] Yongyan Wu,[1,2,3,4] Shuxin Wen,[1,2,3,4] and Binquan Wang[1,2,3,4]

[1]Shanxi Key Laboratory of Otorhinolaryngology Head and Neck Cancer, Taiyuan 030001, Shanxi, China; [2]Department of Otolaryngology Head & Neck Surgery, The First Hospital, Shanxi Medical University, Taiyuan 030001, Shanxi, China; [3]Otolaryngology Head & Neck Surgery Research Institute, Shanxi Medical University, Taiyuan 030001, Shanxi, China; [4]The Key Scientific and Technological Innovation Platform for Precision Diagnosis and Treatment of Head and Neck Cancer, Shanxi Province, Taiyuan 030001, Shanxi, China; [5]Department of Otolaryngology Head & Neck Surgery, Dalian Municipal Friendship Hospital, Dalian 116100, Liaoning, China; [6]Department of Pathology, Shanxi Cancer Hospital, Shanxi Medical University, Taiyuan 030001, Shanxi, China; [7]Department of Otolaryngology Head & Neck Surgery, The First Hospital, Jinzhou Medical University, Jinzhou 121001, Liaoning, China; [8]Department of MRI & CT, Shanxi Cancer Hospital, Shanxi Medical University, Taiyuan 030001, Shanxi, China; [9]Modern Research Center for Traditional Chinese Medicine, Shanxi University, Taiyuan 030001, Shanxi, China; [10]Translational Research Institute, Henan Provincial People's Hospital, School of Medicine, Henan University, Zhengzhou 450053, Henan, China; [11]School of Environmental and Life Sciences, University of Newcastle, Callaghan, NSW 2308, Australia; [12]Translational Medicine Research Center, Shanxi Medical University, Taiyuan 030001, Shanxi, China; [13]Key Laboratory of Cellular Physiology, Ministry of Education, Shanxi Medical University, Taiyuan 030001, Shanxi, China

Laryngeal squamous cell carcinoma (LSCC) is a common form of head and neck cancer with poor prognosis. However, the mechanism underlying the pathogenesis of LSCC remains unclear. Here, we demonstrated increased expression of fascin actin-bundling protein 1 (*FSCN1*) and decreased expression of microRNA-145-5p (miR-145-5p) in a clinical cohort of LSCC. Luciferase assay revealed that miR-145-5p is a negative regulator of *FSCN1*. Importantly, low miR-145-5p expression was correlated with TNM (tumor, node, metastasis) status and metastasis. Moreover, cases with low miR-145-5p/high *FSCN1* expression showed poor prognosis, and these characteristics together served as independent prognostic indicators of survival. Gain- and loss-of-function studies showed that miR-145-5p overexpression or *FSCN1* knockdown inhibited LSCC migration, invasion, and growth by suppressing the epithelial-mesenchymal transition along with inducing cell-cycle arrest and apoptosis. Additionally, hypermethylation of the miR-145-5p promoter suggested that repression of miR-145-5p arises through epigenetic inactivation. LSCC tumor growth *in vivo* could be inhibited by using miR-145-5p agomir or *FSCN1* small interfering RNA (siRNA), which highlights the potential for clinical translation. Collectively, our findings indicate that miR-145-5p plays critical roles in inhibiting the progression of LSCC by suppressing *FSCN1*. Both miR-145-5p and *FSCN1* are important potential prognostic markers and therapeutic targets for LSCC.

INTRODUCTION

Head and neck squamous cell carcinoma (HNSCC) is the sixth most common malignancy worldwide.[1] Laryngeal squamous cell carcinoma (LSCC) has the second highest incidence among these cancers and is especially prevalent in the northern areas of China.[2] The limitations of throat anatomy and the richness of submucous lymph

Received 1 July 2018; accepted 20 September 2018;
https://doi.org/10.1016/j.ymthe.2018.09.018.

[14]These authors contributed equally to this work.

Correspondence: Binquan Wang, MD, Department of Otolaryngology Head & Neck Surgery, The First Hospital Affiliated with Shanxi Medical University, No. 85, South Jiefang Road, Taiyuan 030001, Shanxi, China.
E-mail: wbq_xy@sxent.org
Correspondence: Shuxin Wen, MD, Department of Otolaryngology Head & Neck Surgery, The First Hospital Affiliated with Shanxi Medical University, No. 85, South Jiefang Road, Taiyuan 030001, Shanxi, China.
E-mail: wsxsx@sxent.org
Correspondence: Yongyan Wu, PhD, Department of Otolaryngology Head & Neck Surgery, The First Hospital Affiliated with Shanxi Medical University, No. 85, South Jiefang Road, Taiyuan 030001, Shanxi, China.
E-mail: wuyongyan@sxent.org
Correspondence: Yongping Cui, MD, Translational Medicine Research Center, Shanxi Medical University, Key Laboratory of Cellular Physiology, Ministry of Education, Shanxi Medical University, No. 56, South Xinjian Road, Taiyuan 030001, Shanxi, China.
E-mail: cuiyp@sxmu.edu.cn
Correspondence: Rick F. Thorne, PhD, Translational Research Institute, Henan Provincial People's Hospital, School of Medicine, Henan University, Zhengzhou 450053, Henan, China.
E-mail: rickfthorne@gmail.com

readily facilitate local invasion and neck lymphatic metastasis in LSCC and are important risk factors for recurrence and poor prognosis after treatment. Despite therapeutic advances for many cancer types, the outcomes for most patients with advanced LSCC have not improved significantly in the last 30 years.[3,4] Consequently, understanding the molecular mechanisms of the proliferation, invasion, and metastasis of LSCC is essential for its diagnosis, treatment, and prognosis.

An actin-filament bundling oncogene, fascin actin-bundling protein 1 (*FSCN1*), has been studied in human cancers.[5–7] We previously reported that *FSCN1* was frequently upregulated in LSCC tissues as compared with adjacent normal margin (ANM) tissue. Moreover, upregulation of *FSCN1* was associated with poor prognosis of LSCC.[2] Therefore, understanding the tumor-specific regulation of *FSCN1* is crucial and has potential clinical significance.

MicroRNAs (miRNAs) regulate the expression of protein-coding genes at the post-transcription level, and almost 60% of human genes are thought to be regulated by miRNAs.[8] Dysregulated miRNAs are associated with the malignant progression of LSCC. The functions of miRNAs in LSCC have been revealed. The expression of miR-155 is upregulated in LSCC, and miR-155 overexpression promotes the proliferation and invasion of LSCC by targeting suppressor of cytokine signaling 1 and signal transducer and activator of transcription 3.[9] miR-27a targets polo-like kinase 2 to promote proliferation and suppresses apoptosis in LSCC cells.[10] Conversely, miR-1 overexpression suppresses the migration and invasion of Hep-2 LSCC cells.[11]

Given the critical oncogenic role of *FSCN1* in LSCC, we sought to test whether *FSCN1* expression is regulated by specific miRNAs, with the hypothesis that the regulatory miRNAs could also be crucial for LSCC pathogenesis. We found that miR-145-5p is a negative regulator of *FSCN1* expression in LSCC, and the expression of miR-145-5p was significantly lower in LSCC with poor prognosis. miR-145-5p and *FSCN1* levels affected the phenotypes of LSCC cells, including migration, invasion, colony formation, proliferation, cell-cycle, apoptosis, and tumorigenesis both *in vitro* and *in vivo*. Moreover, miR-145-5p overexpression or *FSCN1* knockdown inhibited the epithelial-to-mesenchymal transitions (EMT) and impaired cytoskeleton organization. Furthermore, miR-145-5p downregulation was attributed to hypermethylation of its promoter.

RESULTS

miR-145-5p Acts as a Negative Regulator of *FSCN1* in LSCC

Our microarray data showed that *FSCN1* was upregulated in LSCC tissues as compared with ANM tissue (Figure 1A), and we previously reported that differentially high expression of *FSCN1* was associated with poor prognosis in LSCC.[2] Furthermore, a recent genome-wide analysis of cancer transcriptomes highlighted that *FSCN1* expression was prognostic in HNSCC.[12] Interrogation of The Cancer Genome Atlas (TCGA) data showed that *FSCN1* was not frequently amplified in LSCC (Figure S1A), and we hypothesized that other regulatory mechanisms were involved, particularly that altered expression of miRNAs and affected *FSCN1* expression in HNSCC. To address this concept, we turned to our prior analysis of miRNA expression profiles in LSCC determined by genome-wide miRNA microarray assay.[13,14]

To determine potential miRNA regulators of *FSCN1*, we performed bioinformatics analysis with miRwalk-2.[15] The miRNAs hit by miRwalk-2 were intersected with miRNAs downregulated in LSCC microarray data (Figure 1B; Tables S1 and S2). Notably, miR-145-5p was the only miRNA that was derived in common with the two approaches (Figure 1C). Therefore, we focused on miR-145-5p as a putative regulator of *FSCN1* in LSCC.

Next, we compared miR-145-5p and *FSCN1* RNA expression across 40 paired samples of fresh LSCC and ANM tissue. For all cases, miR-145-5p was significantly downregulated in LSCC tissue as compared with ANM tissue, and *FSCN1* was differentially upregulated (Figures 1D and 1E). As compared with LSCC cases with low *FSCN1* level, LSCC cases with high *FSCN1* level showed low miR-145-5p level (Figure 1F), with Pearson correlation analyses revealing a clear inverse relation between miR-145-5p expression and *FSCN1* mRNA level ($r = -0.737$; $p < 0.001$) (Figure 1G). In support, *in situ* hybridization experiments illustrated that LSCC lesions with high *FSCN1* level showed low miR-145-5p level (Figure 1H). In contrast, miR-145-5p expression was readily observed in surrounding cells and ANM tissues (Figure 1H; Figure S1B).

To better understand the association between miR-145-5p and *FSCN1*, we used cell models of LSCC (Hep-2 and TU177) along with normal HOK cells for comparison. Notably, qRT-PCR-based analysis demonstrated relatively low expression of miR-145-5p in Hep-2 and TU177 cells, and high level of *FSCN1* as compared with HOK cells showing the reverse pattern (Figure 1I). Moreover, manipulating miR-145-5p levels with a mimic sharply decreased *FSCN1* mRNA and protein levels in both Hep-2 and TU177 cells (Figures 1J and 1K). Together these findings indicate that *FSCN1* expression in LSCC depended on miR-145-5p level, but the underlying basis of this relation remained undefined.

We then sought to determine whether *FSCN1* mRNA was directly regulated by miR-145-5p binding. Indeed, bioinformatics analysis identified that the 3′ UTR region of *FSCN1* contains four putative seed regions with complementarity to miR-145-5p binding (Figure S1C). To verify that miR-145-5p targets *FSCN1* via 3′ UTR-mediated regulation, we conducted experiments with HEK293T cells transfected with *FSCN1* 3′ UTR luciferase reporter constructs. Notably, co-introduction of a miR-145-5p mimic, but not a control, significantly depleted the reporter activity of wild-type *FSCN1* 3′ UTR construct binding (Figure 1L). Similar results were obtained when each of the four miR-145-5p binding sites in the *FSCN1* 3′ UTR construct were individually mutated (Figure 1L). Only mutation of all four miR-145-5p binding sites abrogated the ability of miR-145-5p mimics to inhibit reporter activity (Figure 1L), which suggests that all seed regions participate in *FSCN1* regulation. Overall, these findings support a mechanism whereby miR-145-5p targets *FSCN1*

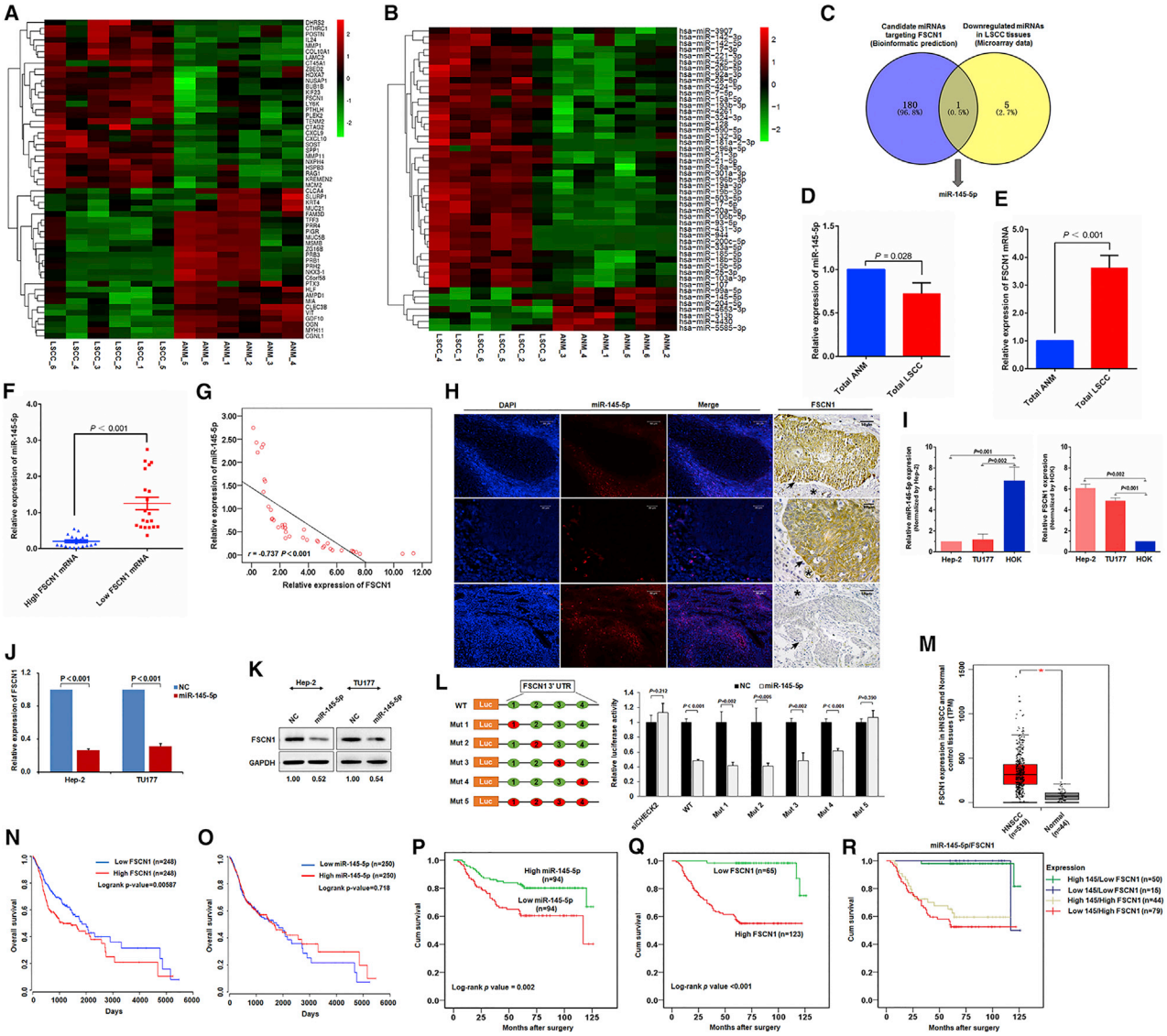

Figure 1. miR-145-5p Is a Negative Regulator of FSCN1 in LSCC and Is Associated with Prognosis of LSCC Patients

Heatmap of (A) mRNAs and (B) miRNAs most increased and decreased in expression in six LSCC tissues as compared with six matched non-tumor tissues analyzed by Arraystar Chip. (C) Screening of miRNA target *FSCN1* in LSCC. Intersection of bioinformatics-predicted miRNAs targeting FSCN1 (181) and miRNAs with decreased expression in LSCC miRNA profiling (6) showing miR-145-5p as a potential negative regulator of FSCN1 in LSCC. (D) miR-145-5p was downregulated in LSCC. qPCR of miR-145-5p level in 40 pairs of fresh LSCC tissue and corresponding ANM tissue. (E) FSCN1 was upregulated in LSCC. qPCR of *FSCN1* level in 40 pairs of fresh LSCC tissue and corresponding ANM tissue. (F) Relative miR-145-5p expression in LSCC tissue with high and low *FSCN1* expression. (G) Pearson correlation analysis of miR-145-5p and *FSCN1* mRNA levels in LSCC tissue. (H) Expression of miR-145-5p and FSCN1 in LSCC tissue determined by fluorescence *in situ* hybridization and immunohistochemical staining. In immunohistochemical staining, black arrows indicate tumor areas, and black stars indicate interstitial tissues. (I) qPCR analysis of RNA levels of miR-145-5p and *FSCN1* in LSCC cells and human oral keratinocyte HOK cells. (J) qPCR analysis of *FSCN1* expression in miR-145-5p mimic-transfected Hep-2 and TU177 cells. (K) FSCN1 protein level in miR-145-5p-transfected Hep-2 and TU177 cells examined by western blot analysis. (L) miR-145-5p binds to the 3′ UTR of *FSCN1* to inhibit its expression. HEK293T cells were co-transfected with luciferase reporter constructs containing wild-type (WT) or mutated *FSCN1* 3′ UTRs and miR-145-5p mimic, and relative luciferase activity was measured and normalized to negative control (NC) mimic-transfected cells. Red circle indicates mutation of miR-145-5p binding site. siCHECK2 indicates cells transfected with the empty vector *psiCHECK-2*, which does not contain the 3′ UTR region of *FSCN1*. (M) Differential expression analysis of *FSCN1* mRNA of head and neck squamous cell carcinoma (HNSCC) patients in the TCGA cohort (tumor group, 519; normal group, 44; *p < 0.01). (N and O) Kaplan-Meier survival curves of HNSCC patients with different FSCN1 (N) and miR-145-5p (O) level in the TCGA cohort via Oncolnc (http://www.oncolnc.org). Upregulated FSCN1 was significantly correlated with poor outcome for patients with HNSCC (log rank test, p = 0.00587), and miR-145-5p level was positively correlated with survival time of HNSCC (log rank test, p = 0.718). (P–R) Kaplan-Meier survival analysis of 188 LSCC patients by expression of miR-145-5p (P), FSCN1 (Q), and a combination of miR-145-5p and FSCN1 (R). p value was determined by log rank test. Error bars represent SD of the indicated clinical samples or three independent assays.

Table 1. Association between Expression of miR-145-5p/FSCN1 and Clinical Features of LSCC Patients

		miR-145-5p Expression		FSCN1 Protein Expression	
Parameters	Cases (n)	Average Rank	p Value[a]	Average Rank	p Value[a]
Age (Years)					
≤60	99	95.92	0.662	88.07	0.038
>60	89	92.92		101.65	
Sex					
Female	21	87.79	0.488	100.14	0.540
Male	167	95.34		93.79	
Primary Cancer Site					
Glottic	101	102.41	0.043	81.40	<0.001
Supraglottic	83	84.87		108.88	
Subglottic	4	94.50		127.00	
Differentiation					
High	72	112.78	<0.001	68.25	<0.001
Medium or low	116	83.16		110.79	
T Staging					
T1+T2	111	105.93	<0.001	87.20	0.007
T3+T4	77	78.02		105.03	
Cervical Lymph Node Metastasis					
N0	142	99.13	0.018	89.27	0.005
N+	46	80.20		110.65	
Distant Metastasis					
M0	183	95.78	0.024	93.61	0.100
M1	5	47.50		127.00	
Clinical Stage					
I+II	96	104.29	0.004	85.88	0.007
III+IV	92	84.28		103.50	
Smoke Preoperatively					
No	75	100.14	0.181	84.39	0.012
Yes	113	90.76		101.21	
FSCN1 Protein Expression					
Low	65	119.81	<0.001	–	–
High	123	81.13		–	

[a]Mann-Whitney U test used for two-group analysis. Kruskal-Wallis H test used for three-group analysis.

directly, and downregulation of miR-145-5p results in *FSCN1* upregulation in LSCC.

Expression of miR-145-5p and FSCN1 Is Associated with Clinical Features and Prognosis in LSCC

To evaluate the clinical and prognostic significance of miR-145-5p expression and FSCN1 protein level in LSCC, we examined their expression in 188 formalin-fixed paraffin-embedded (FFPE) tissue samples (Table S3) by using qRT-PCR and immunohistochemistry. miR-145-5p level was significantly lower in samples from LSCC patients with distant metastases ($p = 0.024$). On multivariate analysis, the expression of miR-145-5p in LSCC tissue was negatively associated with T staging ($p < 0.001$), N status ($p = 0.018$), and clinical stage ($p = 0.004$; Table 1). Conversely, high FSCN1 protein level in LSCC was positively associated with T staging ($p = 0.007$), N status ($p = 0.005$), and clinical stage ($p = 0.007$; Table S4). Moreover, miR-145-5p expression and FSCN1 protein level were inversely related ($p < 0.001$; Table 1).

To examine *FSCN1* expression across HNSCC and normal tissues at the mRNA level, we queried TCGA RNA-sequencing (RNA-seq) data. *FSCN1* mRNA level was markedly higher in HNSCC than normal tissues (Figure 1M). Notably, Kaplan-Meier analysis of TCGA cohorts revealed that upregulated *FSCN1* was significantly associated with poor outcome with HNSCC (Figure 1N). In contrast, HNSCC patients with upregulated miR-145-5p exhibited longer survival time (Figure 1O).

Our analysis revealed better overall survival (OS) in LSCC patients with comparatively high than low level of miR-145-5p (106.09 ± 4.12 versus 85.01 ± 5.24 months; Figure 1P) and poorer OS with high than low level of FSCN1 (79.74 ± 4.43 versus 122.83 ± 1.77 months; Figure 1Q). Subdividing patients into four groups based on miR-145-5p expression and FSCN1 protein level provided an opportunity to further delineate outcomes associated with biological subtype. As expected, LSCC patients with low miR-145-5p/high FSCN1 levels showed low OS, whereas those with high miR-145-5p/low FSCN1 levels showed the best OS (76.98 ± 5.59 versus 123.16 ± 2.03; $p < 0.001$; Figure 1R). Furthermore, on regression analysis, the combination of low miR-145-5p expression and high FSCN1 protein level was an independent prognostic indicator for LSCC survival (relative risk = 12.69; 95% confidence interval [CI] 2.83–56.91; $p = 0.001$; Table S4). Nevertheless, cases with high miR-145-5p/high FSCN1 levels also partitioned with the poor-performing low miR-145-5p/high FSCN1 level cases (Figure 1R). Indeed, FSCN1 level proved to be an independent predictor of LSCC survival (relative risk = 12.27; 95% CI 3.49–43.19; $p = 0.001$; Table S5), although in contrast, miR-145-5p expression alone was not significant in this analysis.

Collectively, these data support the existence of a high-risk biological subtype of LSCC exhibiting low miR-145-5p/high FSCN1 levels, but further propose that high FSCN1 protein level itself is an independent prognostic indicator for LSCC. Thus, we propose that miR-145-5p and its target *FSCN1* are potential biomarkers for the diagnosis and prognosis of LSCC.

Impact of miR-145-5p and *FSCN1* Expression on LSCC Growth and Survival

Next, we sought to better understand the functional impact of miR-145-5p and *FSCN1* expression on the growth behavior of LSCC cells. First, overexpression of miR-145-5p by using mimics in Hep-2 and TU177 cell lines with low endogenous miR-145-5p expression substantially reduced growth and colony formation (Figures 2A and 2B). Measurement of EdU incorporation established reduced cell

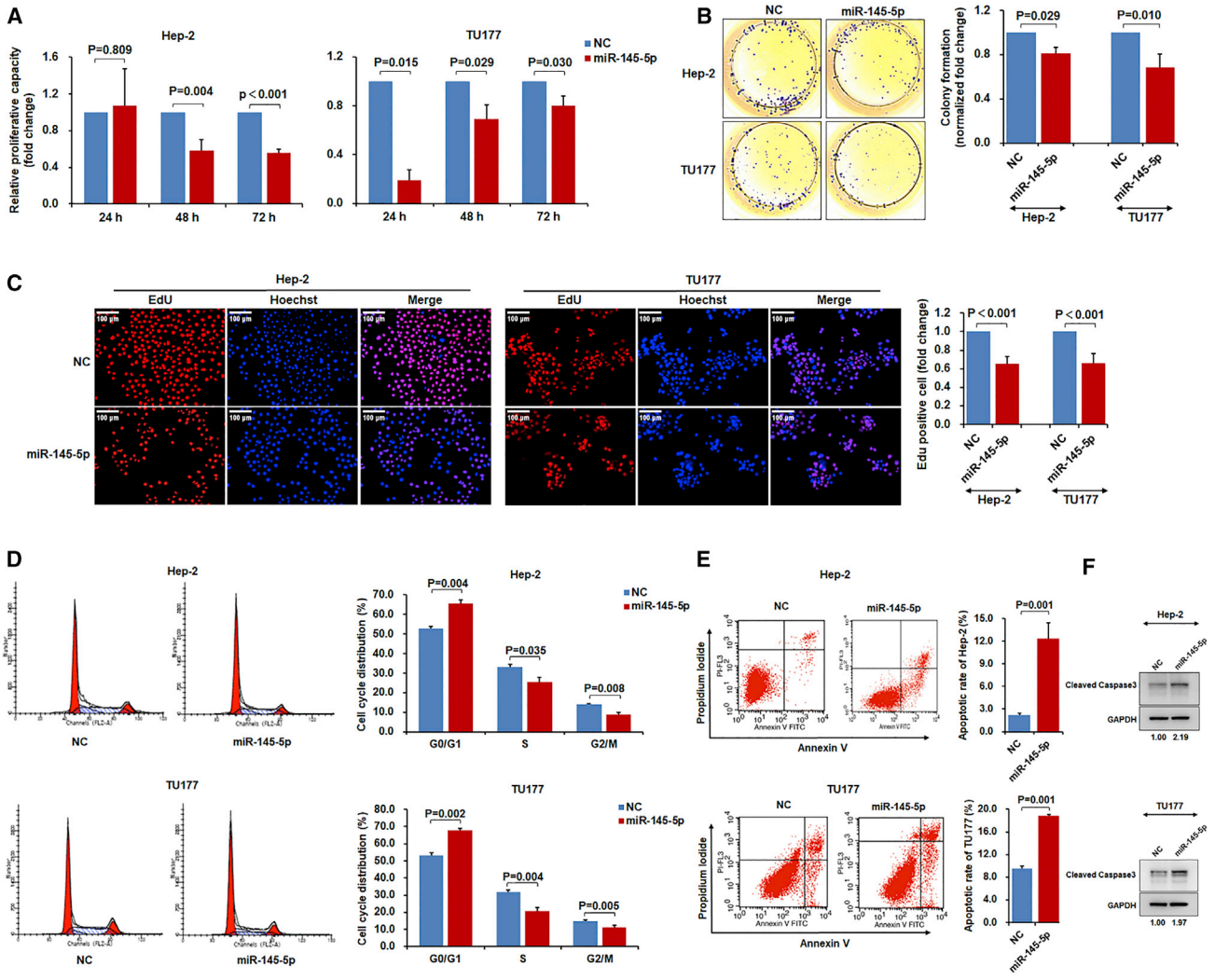

Figure 2. miR-145-5p Inhibits LSCC Cell Proliferation, Colony Formation, and Induces Cell-Cycle Arrest and Apoptosis

Hep-2 and TU177 cells were transfected with miR-145-5p mimic or negative control (NC) mimic for 48 hr. Cell proliferation was measured by cell counting kit-8 analysis (A), colony formation assay (B), and EdU staining (C); cell cycle (D) and apoptosis (E) were measured by flow cytometry. (F) Hep-2 and TU177 cells were transfected with miR-145-5p mimic or NC mimic for 48 hr. Protein level of cleaved caspase-3 was determined by immunoblotting. Data are mean ± SD of three independent experiments. Error bars represent SD of three independent assays.

proliferation rates (Figure 2C), and cell-cycle analyses established that miR-145-5p overexpression increased the proportion of cells in the G0/G1 stage, with concurrent reduction in the S and G2/M stages (Figure 2D). In addition, the proportion of apoptotic cells increased with the introduction of miR-145-5p mimic (Figure 2E). Cells transfected with miR-145-5p showed increased cleavage of caspase-3 and apoptotic bodies, which was consistent with the induction of apoptosis (Figure 2F; Figure S2A). These data indicate that high miR-145-5p expression in LSCC likely inhibits growth by inducing both G0/G1 phase arrest and apoptosis.

We further conducted similar functional analyses after manipulating *FSCN1* levels in LSCC. Both Hep-2 and TU177 cells were depleted of *FSCN1* by using an optimized small interfering RNA (siRNA) protocol (Figure S2B); the reduced FSCN1 protein level was confirmed using immunoblotting (Figure 3A). *FSCN1* knockdown inhibited both cell proliferation and colony formation of Hep2 and TU177 cells (Figures 3B–3D), thereby largely phenocopying the results obtained with the miR-145-5p mimic. In accordance with these data, *FSCN1* knockdown pushed cells toward the G0/G1 phase (Figure 3E) and increased the proportion of cells undergoing apoptosis (Figure 3F). Moreover, immunoblotting results showed that *FSCN1* knockdown increased cleavage of caspase-3 (Figure 3G). Thus, these effects of miR-145-5p and *FSCN1* in LSCC *in vitro* reconcile well with the clinical behavior of LSCC tumors *in vivo*.

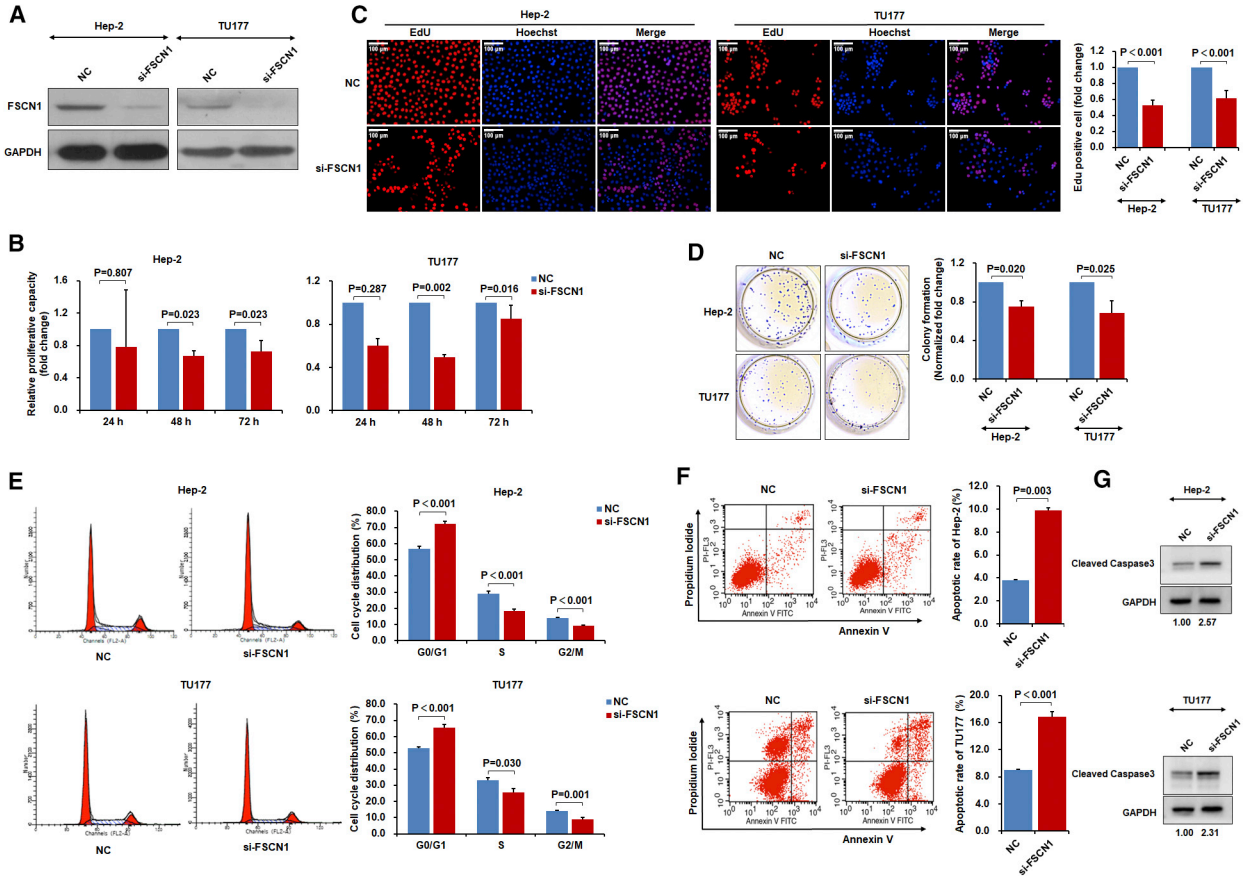

Figure 3. *FSCN1* Knockdown Inhibits LSCC Cell Proliferation and Induces Cell-Cycle Arrest and Apoptosis

Hep-2 and TU177 cells were transfected with siRNA targeting *FSCN1* (si-*FSCN1*) or negative control (NC) for 48 hr, and *FSCN1* levels were determined by western blot assay (A). Assays of cell proliferation (B), EdU staining (C), colony formation (D), cell cycle (E), and apoptosis (F) after indicated treatments. (G) Hep-2 and TU177 cells were transfected with si-*FSCN1* or NC for 48 hr. Protein level of cleaved caspase-3 was determined by immunoblotting. Data are mean ± SD of three independent experiments. Error bars represent SD of three independent assays.

The miR-145-5p/*FSCN1* Regulatory Axis Controls the EMT in LSCC

In addition to having effects on cell proliferation and survival, the miR-145-5p mimic appeared to affect the adhesive properties of LSCC cells (Figure S2C). Given the well-known relation between cell adhesion and motility migration, we further investigated this phenomenon. Indeed, overexpression of miR-145-5p with a mimic significantly inhibited cell migration and invasion in Transwell assays as compared with controls (Figures 4A and 4B). Consistent with the mechanistic relation uncovered between miR-145-5p and *FSCN1*, on repeating these assays with *FSCN1* siRNA, Hep-2 and TU177 cells showed decreased migration and invasion (Figures 4C and 4D). Hence our findings propose that *FSCN1* is an oncogene in LSCC that promotes cell proliferation and is also involved in promoting migration and invasion.

A corollary to these findings was the phenotype of LSCC cells observed by scanning electron microscopy. Control cells showed the typical morphology of cultured cancer cells with prominent lamellipodial and filopodial structures, whereas LSCC cells treated with miR-145-5p mimic or si-*FSCN1* showed very few lamellipodia and filopodia, for a relatively rounded cell morphology (Figure 4E). Furthermore, impaired F-actin polymerization and filopodium formation were observed after miR-145-5p restoration or *FSCN1* knockdown (Figure 4F). Hence, the miR-145-5p/*FSCN1* mechanism may be involved in controlling the EMT in LSCC, generally known as a critical determinant of tumor cell metastasis.[16]

To determine whether the regulation of *FSCN1* expression via miR-145-5p and consequent modulation of migration and invasion of LSCC depended on the EMT, we analyzed EMT marker expression. Immunoblotting of Hep-2 and TU177 LSCC cells treated with miR-145-5p mimic or with *FSCN1* siRNA revealed increased expression of E-cadherin level along with reduced levels of Vimentin, Snail, N-cadherin, and matrix metalloproteinase 2 (MMP2) and matrix metalloproteinase 9 (MMP9) (Figures 4G and 4H). Hence, miR-145-5p inhibited the EMT, and its target, *FSCN1*, promoted the EMT in LSCC.

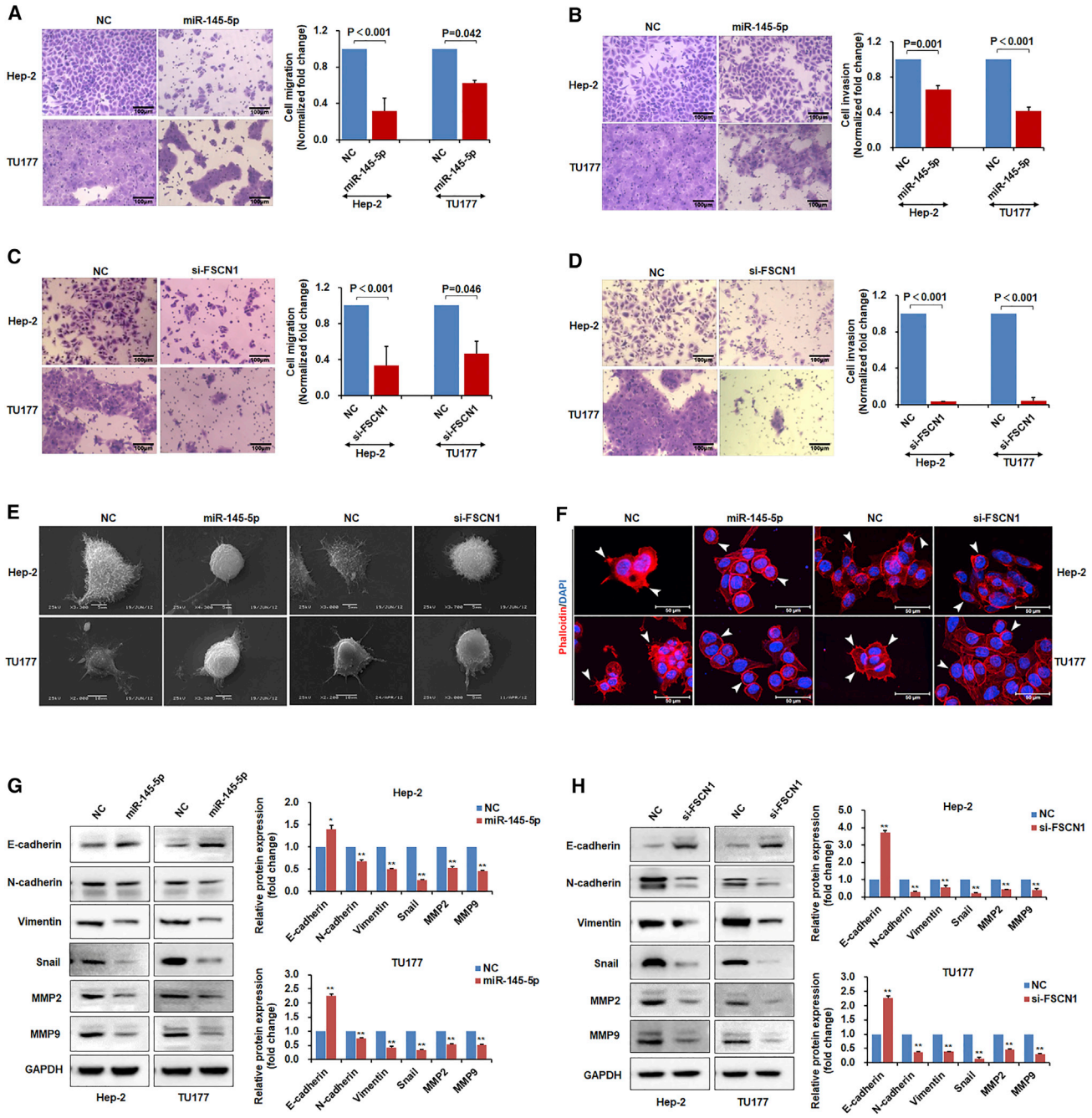

Figure 4. miR-145-5p Overexpression or *FSCN1* Knockdown Inhibits LSCC Cell Migration, Invasion, and Endothelial-to-Mesenchymal Transition

Hep-2 and TU177 cells were transfected with miR-145-5p mimic or si-*FSCN1* for 48 hr. (A and C) Cell migration of miR-145-5p overexpressed (A) and FSCN1 knockdown (C) cells were measured by Transwell assays. (B and D) Cell invasion of miR-145-5p overexpressed (B) and FSCN1 knockdown (D) cells were measured by Transwell assays. (E) Surface structure of cells was observed by scanning electron microscopy. (F) F-actin was stained with rhodamine phalloidin, and nuclei were stained with DAPI. As indicated by white arrows, miR-145-5p mimic or si-FSCN1 treatment decreased cell lamellipodial and filopodial structures as compared with the NC. (G and H) Expression of EMT markers E-cadherin, N-cadherin, Vimentin, Snail, MMP2, and MMP9 in miR-145-5p overexpressed (G) and FSCN1 knockdown (H) cells were determined by western blot assays. Representative images and data from three independent experiments. Data are mean ± SD of three independent experiments. Error bars represent SD of three independent assays. *$p < 0.05$, **$p < 0.01$.

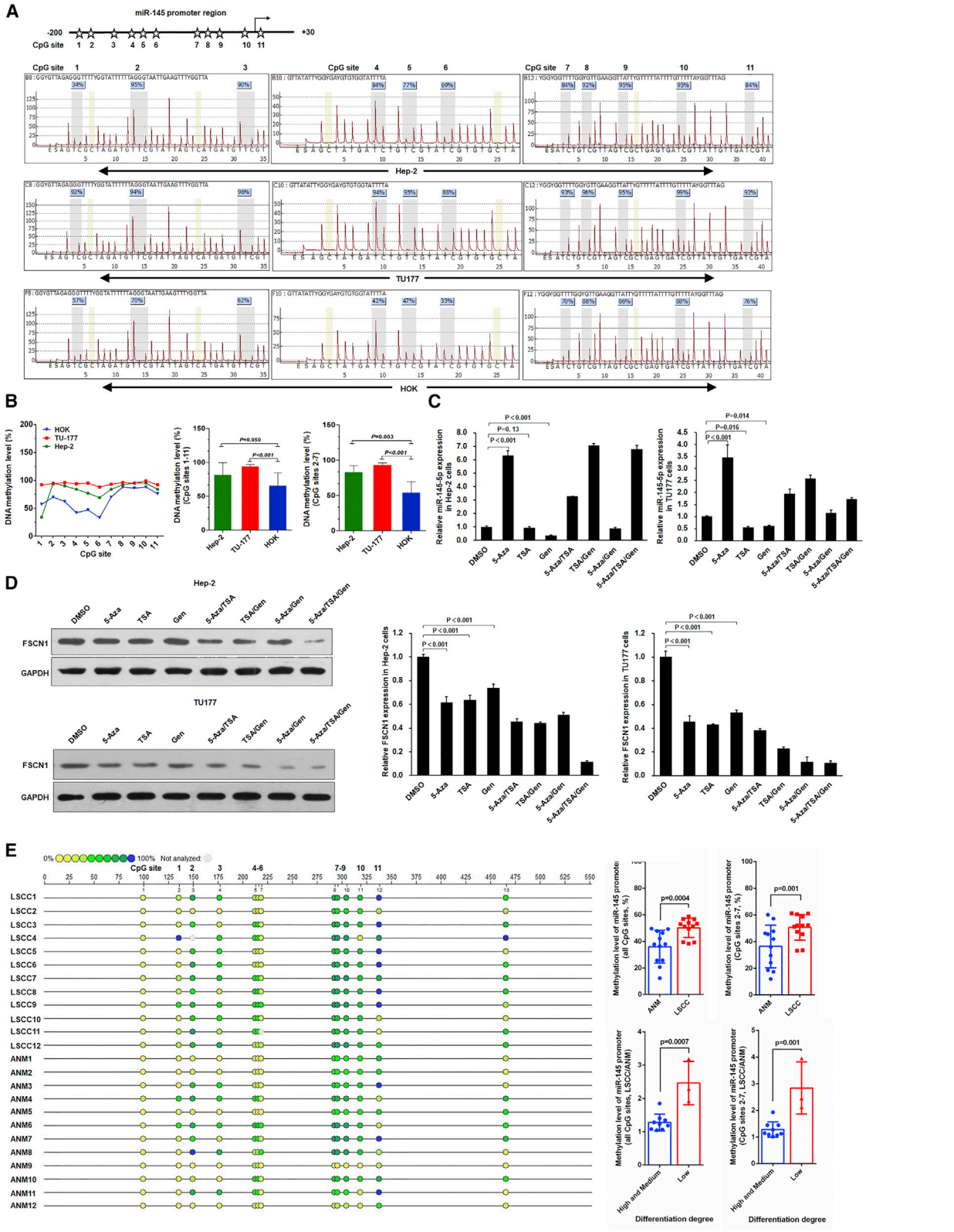

(legend on next page)

Expression of miR-145-5p Is Regulated by Promoter Hypermethylation in LSCC

A final question remained as to why downregulation of miR-145-5p occurs in the malignant transition of LSCC cells. To understand this, we analyzed the DNA methylation of the miR-145-5p proximal promoter in LSCC cell lines by using pyrosequencing. As compared with normal control HOK cells, in Hep-2 and TU177 LSCC cells, the CpG sites 2–7 were highly methylated (Figures 5A and 5B), which suggests that promoter hypermethylation underpinned the loss of miR-145-5p expression in LSCC. In support, miR-145-5p expression was significantly increased in Hep-2 and TU177 cells treated with the DNA methyltransferase inhibitor 5-Aza-deoxycytidine (5-Aza) (Figure 5C). In addition, we tested the effect of the histone deacetylase inhibitor trichostatin A (TSA) and chemopreventive agent genistein on miR-145-5p expression. TSA and genistein alone inhibited miR-145-5p expression, whereas their combination increased miR-145-5p expression. Cells treated with 5-Aza combined with TSA and/or genistein showed increased miR-145-5p expression (Figure 5C). Endogenous FSCN1 protein expression exhibited corresponding changes in 5-Aza-treated Hep-2 and TU177 cells (Figure 5D). Notably, genistein treatment reduced both miR-145-5p level and FSCN1 protein level (Figure 5D), which might be due to its different regulatory pathways for miR-145-5p and FSCN1. Moreover, by MassARRAY methylation analysis, we determined the DNA methylation level of miR-145-5p promoter in clinical LSCC tissues separated by laser capture microdissection (LCM) (Figure S3). The methylation level of the miR-145-5p promoter was significantly higher in LSCC tissue than paired ANM tissue (Figure 5E), and the methylation level of the miR-145-5p promoter was inversely associated with the differentiation degree of LSCC (Figure 5E). Together these findings propose that promoter hypermethylation underpins the low expression of miR-145-5p observed in LSCC.

miR-145-5p Suppresses LSCC Tumor Growth *In Vivo* in a Preclinical Model

To establish the proof of principle that modulating miR-145-5p or *FSCN1* expression in LSCC could be an effective therapy, we used a xenograft model. Subcutaneous (s.c.) tumors of Hep-2 or TU177 LSCC cells were established in opposing flanks of nude mice and allowed to grow to 0.5 mm^3. Thereafter, miR-145-5p agomir or control (negative control [NC]) agomir was intra-tumorally injected, and tumor growth was monitored over 4 weeks. Compared with controls, injection of miR-145-5p agomir significantly decreased tumor growth rates and tumor size (Figure 6A). Consistent with previous experiments, injecting tumors with *FSCN1*-targeting oligos also decreased the growth rate and tumor weight of Hep-2 and TU177 tumors (Figure 6B). Moreover, histopathological examination of tissues from miR-145-5p or *FSCN1* siRNA-injected tumors showed a higher abundance of shrunken and fragmentized nuclei in sections as compared with control tissues (Figure 6C), which suggests increased rates of apoptosis. This finding was confirmed on TUNEL assay, whereby miR-145-5p overexpression or *FSCN1* knockdown increased cell apoptosis as compared with controls (Figure 6D).

Further analysis of xenografted LSCC tissues by immunohistochemical staining confirmed that the injection of both miR-145-5p agomir and *FSCN1* siRNA decreased FSCN1 protein level (Figure 6E). Moreover, the expression of cyclin-D1 and the proliferation marker Ki67 was decreased in tumors with miR-145-5p agomir and *FSCN1* siRNA injection (Figure 6E). Furthermore, as compared with controls, tumors with miR-145-5p agomir or *FSCN1* siRNA injection showed upregulated E-cadherin and downregulated MMP2 and MMP9 (Figure 6F). Thus, we established the proof of principle that modulating miR-145-5p expression *in vivo* could inhibit LSCC tumor growth ostensibly via the same mechanisms revealed in *in vitro* experiments.

DISCUSSION

The prognostic value of *FSCN1* expression has previously emerged across a number of cancer types, with its upregulation known to promote migration and invasion.[17,18] Our previous study involving LSCC found FSCN1 protein overexpression associated with clinical features and poor prognosis.[2] However, the regulatory mechanisms of *FSCN1* in LSCC remain undefined. In the present study, we found that miR-145-5p functioned as a negative regulator of *FSCN1* in LSCC tissue and cells, with decreased miR-145-5p level and accompanying increased *FSCN1* level acting as critical determinants of poor prognosis. miR-145-5p and *FSCN1* levels may have potential for predicting outcomes with LSCC. Indeed, their applicability as novel biomarkers to identify LSCC patients with distinct clinical features is underscored by our findings relating miR-145-5p expression and FSCN1 protein level with tumor, node, metastasis (TNM) and clinical staging. Moreover, we demonstrated that miR-145-5p has an important regulatory role in LSCC, inhibiting LSCC cell proliferation along with the accompanying cell-cycle arrest and apoptosis. Nevertheless, we also found evidence of a high-risk LSCC group displaying elevated miR-145-5p level with high FSCN1 protein level, likely indicating that non-miR-145-5p mechanism(s) are also responsible for high FSCN1 protein level in some cases.

Figure 5. Hypermethylation of miR-145-5p Promoter Suppresses miR-145-5p Expression in LSCC Cells

(A and B) Pyrosequencing analysis of miR-145-5p promoter methylation status in LSCC cell lines Hep-2 and TU177 and normal control HOK cells. The methylation level in Hep-2 and TU177 cells was normalized to that in HOK cells. Pyrosequencing map (A) and statistical results (B) of methylation levels of Hep-2, TU177 and HOK cells. (C) Hep-2 and TU177 cells were treated with 5-Aza, trichostatin A (TSA), and genistein (Gen) as indicated; the expression of miR-145-5p was determined by qPCR. (D) Hep-2 and TU177 cells were treated with 5-Aza, TSA, and Gen as indicated; *FSCN1* protein level was measured by western blot assay. Data are mean ± SD of three independent experiments. (E) Methylation analysis of miR-145-5p in clinical LSCC and paired ANM tissues. DNA purified from LSCC and paired ANM tissues by laser capture microdissection was treated with bisulfite and subjected to MassARRAY methylation analysis. Error bars represent SD of the indicated clinical samples or three independent assays.

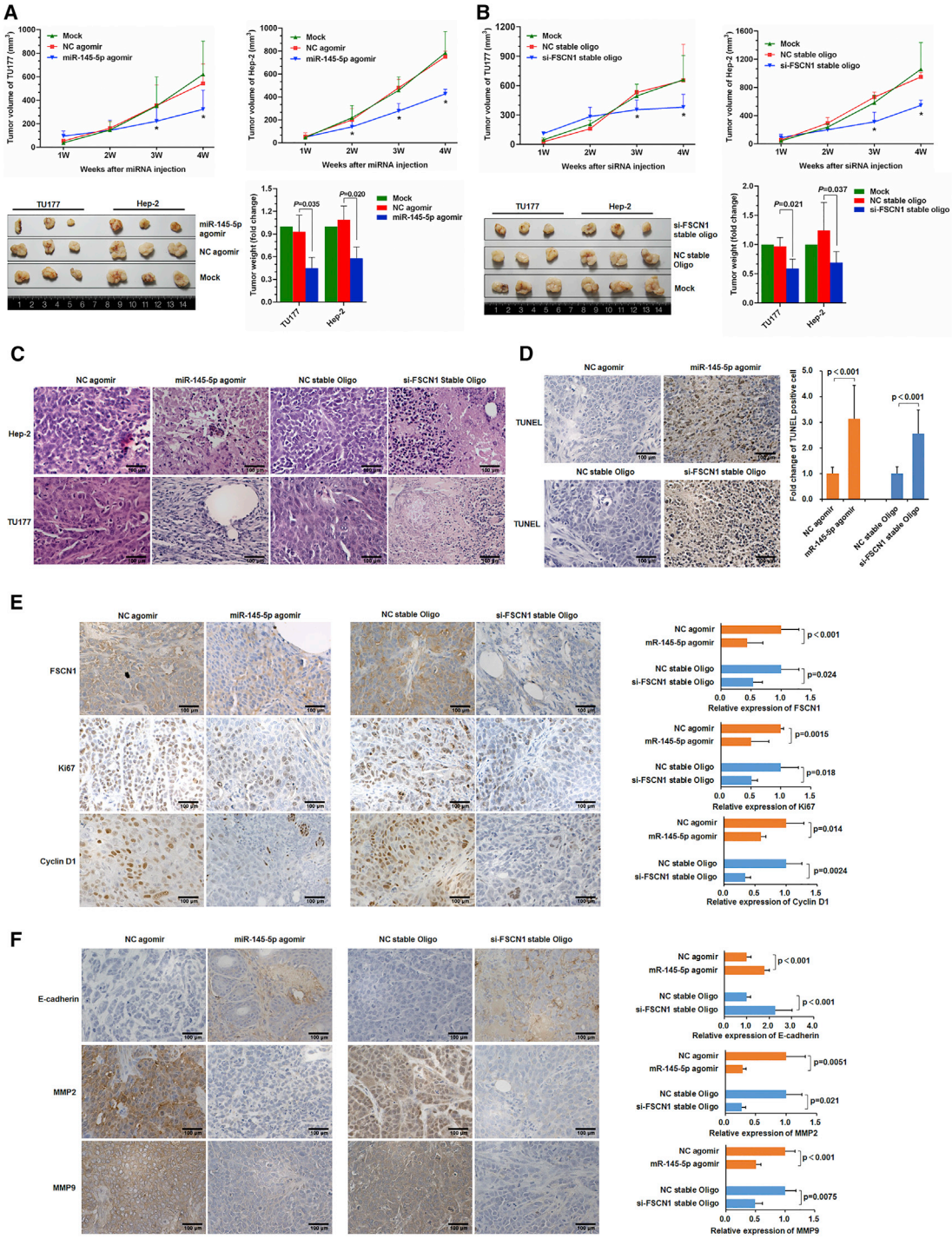

Figure 6. miR-145-5p Overexpression or *FSCN1* Knockdown Inhibits LSCC Xenograft Tumor Formation in Mice

Nude mice were subcutaneously injected with Hep-2 and TU177 cells. After tumor formation, miR-145-5p agomir, NC agomir, si-*FSCN1* stable oligonucleotides, and corresponding negative oligonucleotides were subcutaneously injected into tumor sites. Tumor volume and weight after injection of miR-145-5p agomir (A) or si-*FSCN1* (B) were plotted. Data are mean ± SD. *$p < 0.05$. (C) Representative H&E staining images of Hep-2 and TU177 xenograft tumors. (D) TUNEL assay of apoptotic cells in xenograft tumors. (E) Representative immunohistochemical staining of *FSCN1* and proliferation markers Ki67 and CyclinD1 in Hep-2 and TU177 xenograft tumors. (F) Representative immunohistochemical staining of EMT markers E-cadherin, MMP2, and MMP9 in xenograft tumors. Data are mean ± SD of three independent experiments. Error bars represent SD of three independent experiments.

We initiated our study in response to the clinical impact of *FSCN1* expression in LSCC. After identifying miR-145-5p by a bioinformatics approach, we sought to learn more about its role and mechanisms, particularly involving LSCC. We now provide definitive evidence that miR-145-5p robustly targets *FSCN1* via a multivalent mechanism involving all four binding sites identified within the 3′ UTR of *FSCN1* mRNA. However, although we demonstrated that inhibiting *FSCN1* expression in LSCC largely reproduced the experimental findings observed when miR-145-5p expression was restored, we cannot exclude the involvement of other important targets. Indeed, a previous study suggested that miR-145-5p acts in LSCC cells to inhibit stem cell markers SRY-box 2, POU class 5 homeobox 1 (also known as OCT4), Kruppel-like factor 4, and ATP binding cassette subfamily G member 2,[19] although the mechanisms need to be further investigated. More generally, these findings expand on the growing evidence of the importance of the miR-145 locus in cancer progression.[20–23]

miR-145-5p is found within a cluster of "dual-stranded" miRNAs that also include miR-143-3p, miR-145-3p, and miR-143-5p.[24] Recent evidence obtained in colorectal cancer,[25] along with prostate cancer,[26] has highlighted that miR-145-5p can target *FSCN1* with tumor-suppressive effects on cancer cells. Studies have established the role of several other miRNAs in the 143/145 cluster as tumor suppressors. Moreover, miR-143-5p deficiency in gallbladder cancer triggered the EMT and metastasis by targeting HIF-1α in mesothelioma.[27] miR-143-3p suppresses the progression of ovarian cancer and esophageal squamous cell carcinoma,[28,29] and miR-145-3p acts as a tumor suppressor in HNSCC by targeting *MYO1B*.[30] Despite some evidence that miRNAs in the 143/145 group may be co-regulated,[31] in the context of the current work, we did not evaluate the expression of miRNAs other than miR-145-5p, given our focus on *FSCN1*. Evaluating the overall impact of each miRNA in the 143/145 cluster on cancer biology is pertinent, as is understanding the hierarchy of their regulatory relationships.

What are the clinical implications of our work? Both *in vitro* and *in vivo* experiments demonstrated that miR-145-5p overexpression or *FSCN1* knockdown suppressed tumor growth of LSCC via effects on proliferation and cell survival. Notably, using the *in vivo* models in nude mice, we established that direct injection of miR-145-5p agomir or stable si-*FSCN1* oligonucleotides into the tumor significantly retarded growth. This procedure differs from a previous method of directly injecting miRNA-overexpressing cancer cells into nude mice.[32] However, our method simulated the process of drug therapy in clinical practice and highlighted the significance of miR-145-5p and *FSCN1* as targets of LSCC therapy.

In addition to the effects observed on proliferation and survival, a further biological effect of suppressing miR-145-5p expression in LSCC involved maintaining the cells in a high motility state. Here the re-introduction of miR-145-5p and likewise antagonizing *FSCN1* expression inhibited cell migration and invasion with a drastic alteration in cell phenotype. Both miR-145-5p-agomir and si-*FSCN1*-treated cells lost protrusive structures (lamellipodia, filopodia, and invadopodia) associated with migrating and invading cells. Such structures are formed by spatiotemporal-regulated actin polymerization at the leading edge of the migratory cells, with aberrant regulation leading to malignant progression such as tumor invasion and metastasis.[33,34] Moreover, increased cellular protrusions have been shown to promote invasion and metastasis in oral squamous carcinoma.[35] Because FSCN1 is involved in F-actin crosslinking and cytoskeletal organization during cell motility,[36–38] the inhibitory effects on FSCN1 expression may explain how miR-145-5p acts to suppress LSCC migration and invasion.

The EMT plays a crucial role in increased invasion, metastasis, and proliferation for carcinoma. When EMT occurs, the expression of an epithelial marker, such as E-cadherin, is suppressed, whereas that of mesenchymal markers, such as N-cadherin, Vimentin, Snail, MMP2, and MMP9, are enhanced.[39] Altering the expression of miR-145-5p and its target, *FSCN1*, caused EMT reversal in LSCC, as shown by the increased expression of E-cadherin and reduced expression of N-cadherin, Vimentin, Snail, MMP2, and MMP9 both *in vitro* and in LSCC tumors *in vivo*. These findings imply that the associated phenotypic and functional changes in LSCC accompanying loss of miR-145-5p are associated with the process of EMT. The EMT of cancer cells accompanies the formation of invasive structures such as lamellipodia and filopodia. These changes depend on the reorganization of actin cytoskeleton, and actin-associated proteins control the polymerization and depolymerization processes to regulate the reorganization of actin cytoskeleton.[40,41] Moreover, recent studies revealed that the actin binding protein Cofilin 1 (*CFL1*) promotes the EMT process by promoting the formation of invasive structures, as well as by modulating EMT-related gene expression via regulation of actin organization in the nucleus.[42] The present results demonstrate that FSCN1 knockdown inhibits invadopodia formation and impairs actin cytoskeleton organization. Therefore, we hypothesized that FSCN1 affects EMT-related gene expression by regulating actin cytoskeleton organization. Further studies are required to elucidate how miR-145-5p/*FSCN1* regulates the EMT pathway.

Finally, as observed in some other cancer types,[43] we found a differentially lower expression of miR-145-5p in LSCC versus normal tissues. Given the role of miR-145-5p as a tumor suppressor, our study also investigated how its expression is suppressed in LSCC. Promoter-region hypermethylation causing silencing of miR-145-5p was previously observed in cancer,[44] and our data similarly support a differentially increased methylation of the miR-145-5p promoter region in LSCC as compared with normal tissues, and high methylation levels of the miR-145-5p promoter indicated low differentiation of LSCC. This observation was functionally evaluated by treating LSCC cells with a variety of epigenetic modifier compounds, with our findings indicating that miR-145-5p expression in LSCC could be readily restored by a number of different treatment approaches. Moreover, consistent with the proposed mechanism (Figure 7), we found largely concurrent reduced expression of *FSCN1*. However, our findings are not fully concordant with previous data; for example, we found that treatment with TSA plus genistein potently upregulated

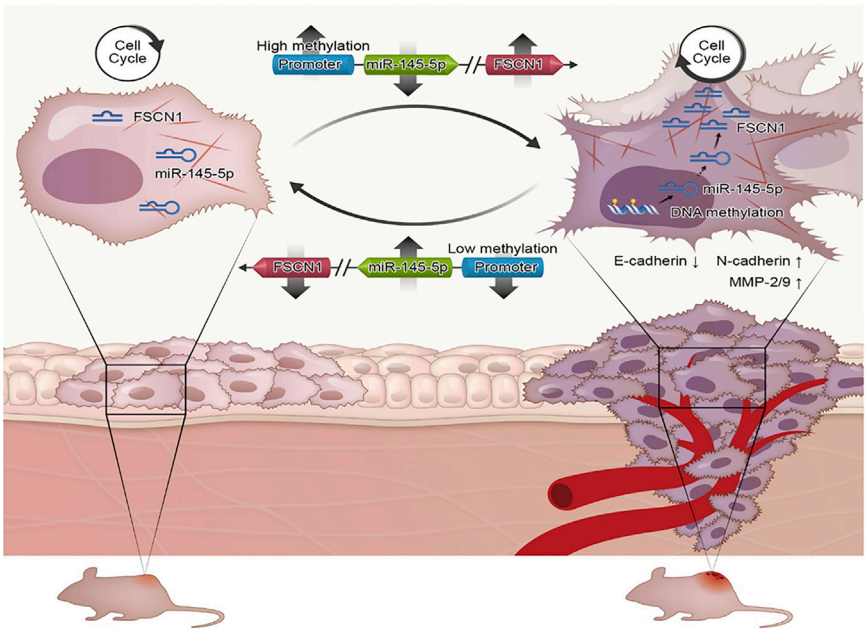

Figure 7. Proposed Regulatory Model for miR-145-5p/*FSCN1* Axis in LSCC Progression

Expression of miR-145-5p was silenced by hypermethylation of its promoter in LSCC. miR-145-5p inhibits malignant phenotypes of LSCC by directly targeting *FSCN1* to inhibit the EMT and cytoskeletal organization. Downregulation of miR-145-5p upregulates *FSCN1* in LSCC, thus promoting tumorigenesis and progression.

miR-145-5p expression in LSCC cells, which contrasts with previous data in prostate cancer cells.[45] We need to understand the effects of these agents in different cell contexts. Regardless, our findings highlight the potential for these approaches to reverse the methylation of the miR-145-5p promoter region as a potential treatment avenue for LSCC.

MATERIALS AND METHODS

Ethical Statement

This study was conducted in accordance with the Helsinki Declaration. All patients signed a written, informed consent before surgery, acknowledging that they understood their rights and obligations. Animal studies were carried out in compliance with our institutional guidelines, and animal experimental procedures were approved by the Animal Care Commission of Experimental Animal Center of Shanxi Medical University. All aspects of the study were approved in full by the Research Ethics Committee at Shanxi Medical University.

Clinical Samples and Patient Population

Forty LSCC tissues and 40 corresponding ANM tissues were obtained from patients undergoing surgery in the Department of Otolaryngology Head & Neck Surgery, The First Hospital Affiliated with Shanxi Medical University. ANM tissues were isolated from surgical specimens at about 1–3 cm from the neoplastic edge. Fresh specimens were frozen by use of liquid nitrogen for qRT-PCR and western blot analysis, and the other part was embedded in paraffin for H&E staining to ensure the diagnosis of LSCC and ANM.

Study Participants

The study involved 188 LSCC patients undergoing surgery in our department from 2000 to 2006. Patients did not receive radiotherapy or chemotherapy before surgery and were without prior associated clinical treatment before diagnosis. The dates of laryngeal cancer surgery and of last follow-up and status at last follow-up (living, lost to follow-up, or deceased) were recorded. Two staff anatomical pathologists provided the diagnosis of laryngeal cancer from paraffin-embedded tissues. Tumor and clinical staging involved the TNM staging system of the American Joint Committee on Cancer (2010). The histological types of LSCC were determined according to the World Health Organization system. Detailed clinical records were available for all participants with follow-up records at three monthly intervals (phone, mail, or outpatient visit) with the final recording in November 2011. Survival time was defined as the time between the date of surgery and patient death or the end of the study period.

Cell Culture and Transfection

The human 293T and LSCC cell line Hep-2 was purchased from the China Center for Type Culture Collection and cultured in DMEM (GIBCO, Grand Island, NY, USA) supplemented with 10% fetal bovine serum (FBS) (BI, Cromwell, CT, USA). TU177 cells (Bioleaf Biotech, Shanghai) were cultured in MEM supplemented with 10% FBS. Normal human oral mucous-membrane keratinizing basal cells (HOK) were cultured with ScienCell OKM (Cat. No. 2611; ScienCell) and 10% FBS. The micrON Hsa-miR-145-5p mimic (miR10000437-1-5) was from RiboBio (Guangzhou, China) and used in cell transfection experiments. The siRNA and NC were from Genechem (Shanghai). Cells were transfected with Lipofectamine 2000 following the manufacturer's instructions. *FSCN1* siRNA sequences were for si-*FSCN1*-1: 5′-CGACTATAACAAGGTGGCCAT-3′, si-*FSCN1*-2: 5′-CAAAGACTCCACAGGCAAA-3′, and si-*FSCN1*-3: 5′-CAAGTTTGTGACCTCCAAGAA-3′. 5-Aza, TSA, and Genistein were from Sigma-Aldrich (St. Louis, MO, USA) and were dissolved in DMSO. Cells with 50%–60% confluence were treated with concentrations of 5-Aza (10 μM), TSA (100 ng/mL), and Genistein (25 μM); cells treated with DMSO were controls.

DNA Methylation Analysis

For cell sample, DNA was extracted and treated with bisulfite by using the EpiTect Bisulfite Kit (QIAGEN, Germany). An amount of 2 μL of bisulfite-treated DNA was used for PCR to amplify the miR-145

promoter fragment with primers listed in Supplemental Materials and Methods. After purification, PCR products were degenerated for 2 min with the sequencing primer (Supplemental Materials and Methods) at 80°C, followed by pyrosequencing on the PyroMark Q96 instrument (QIAGEN, Germany).

For clinical samples, to precisely separate the tumor and normal tissue frozen sections, we stained frozen sections of LSCC or paired ANM fresh tissue with Histogene staining solution (Thermo Fisher Scientific, Waltham, MA, USA) and microdissected them by using the Leica LMD6500 laser microdissection system (Leica Microsystems CMS, Wetzlar, Germany). DNA was extracted from the microdissected LSCC and ANM tissue fragments. Subsequently, MALDI-TOF-mass spectrometry (MS)-based DNA methylation analysis was performed with MassARRAY Analyzer 4.0 (Agena Bioscience, San Diego, CA, USA) as described previously.[46] In brief, the target gene regions were amplified by using bisulfite-modified DNA and the primer pairs described in the Supplemental Materials and Methods. Next, *in vitro* RNA transcription was performed on the reverse strand, followed by base-specific cleavage. The cleavage products were analyzed by using MALDI-TOF, and a distinct signal pair pattern resulting from the methylated and non-methylated template DNA was obtained and analyzed by using MassARRAY EpiTYPER (Agena Bioscience, San Diego, CA, USA). The clinical features of LSCC samples that underwent MassARRAY methylation analysis are described in Table S6.

Nude Mouse Xenograft Tumor Model

BALB/C nude mice (specific pathogen-free grade, female, 7 weeks old) were obtained from HNJIA (Hunan, China). Mice were maintained in the Medical Experimental Animal Center (Guangzhou, China). Hep-2 or TU177 cells were s.c. injected into the flanks of nude mice to generate xenograft tumors. Agomir is a chemically modified double-strand miRNA mimic, with two phosphorothioates at the 5′ end, four phosphorothioates and one cholesterol group at the 3′ end, and a full-length nucleotide 2′-methoxy added to the antisense strand. Compared with miRNA mimics, agomir exhibits enhanced cellular uptake, stability, and regulatory activity *in vivo*. Agomir can upregulate corresponding miRNAs by local or systemic injection into animals. Hsa-miR-145-5p agomir and *FSCN1* siRNA stable oligonucleotides modified by cholesterol, 2′-OMe, and phosphorothioate were synthesized by GenePharma (Shanghai). When tumors had grown to 0.5 mm^3, miR-145-5p agomir and *FSCN1* siRNA stable and NC oligonucleotides were s.c. injected into the tumor site as follows: multi-point injection with 0.1 mL oligonucleotides (10 nmol), 2 times/week/position and on the first and fourth day per week. The delivery efficiency and distribution of miR-145-5p agomir or FSCN1 siRNA in tumors were verified (Figure S4). Tumor growth was measured every week. Tumor volume (V) was calculated as $V = (L \times W^2)/2$. Four weeks after the first injection, mice were euthanized, and tumors were excised, weighed, and paraffin embedded.

Statistical Analysis

Statistical analysis involved use of SPSS v19.0 (SPSS, Chicago, IL, USA) and R software v3.2.5 (https://www.r-project.org/). Independent Student's t test was used to compare the differences between two groups. The association between miR-145-5p/FSCN1 expression and clinicopathological variables was assessed by Pearson's chi-square or Fisher's exact test. Mann-Whitney test was used for two-group analysis, and Kruskal-Wallis test for three-group analysis. The association between miR-145-5p and FSCN1 RNA expression in clinical samples was assessed by Pearson correlation analysis. OS was defined as the time from surgery date to death from laryngeal carcinoma or date of last contact. Survival was analyzed by the Kaplan-Meier method with a log rank test. Eight possible factors affecting LSCC selected to analyze by Cox proportional-hazards regression included age, T staging, neck lymph node metastasis, differentiation level, clinical stage, smoking preoperatively, miR-145-5p expression, and FSCN1 protein expression. The reported results included relative risk and 95% CIs for all tests. Two-sided $p \leq 0.05$ was considered statistically significant.

The following experiments were presented in the Supplemental Materials and Methods: RNA extraction and qRT-PCR analysis, western blot analysis, generation of reporter constructs, luciferase reporter assay, immunohistochemistry staining and analysis, cell proliferation assay, cell adhesion assay, apoptosis analysis, cell-cycle analysis, Transwell migration/invasion assay, microscopy imaging, and staining. Antibody information is shown in the Supplemental Materials and Methods.

SUPPLEMENTAL INFORMATION

Supplemental Information includes four figures, six tables, and Supplemental Materials and Methods and can be found with this article online at https://doi.org/10.1016/j.ymthe.2018.09.018.

AUTHOR CONTRIBUTIONS

B.W., S.W., Y.W., Y.C., R.F.T., and W.G. conceived the study and participated in the study design; W.G., C.Z., H. Li, W.L., J.S., X.Z., H. Luo, Y.L., Y.S., D.Y., R.Z., Z.L., Y.B., H.G., J.W., M.N., J.H., Z.W., and C.X. developed methods and performed the experiments; C.Z., Q.Z., Y.B., and R.Z. obtained clinical samples and data; W.G., X.Z., H. Luo, J.S., W.L., and Y.W. performed bioinformatics analysis; W.G., C.Z., H. Li, Y.C., and L.Z. analyzed experimental data; W.G., R.F.T., Y.Y.W., S.X.W., and B.Q.W. wrote the manuscript; Y.Z., J.C., and J.L. repeated the experiments. All authors read and approved the final manuscript.

CONFLICTS OF INTEREST

The authors have no conflicts of interest.

ACKNOWLEDGMENTS

This work was supported by the National Natural Science Foundation of China (grants 81602394, 81402256, and 81572670), China Postdoctoral Science Foundation (grants 2016M591412 and 2017M610174), Natural Science Foundation of Shanxi Province (grants 2014011039-5, 2015021198, and 201601D011087), Shanxi Province Scientific and Technological Achievements Transformation Guidance Foundation (grants 201604D131002 and 201604D132040),

Key Technological Innovation Platform Foundation for Head and Neck Cancer Research of Shanxi Province (grant 201605D151003), Scientific and Technological Innovation Programs of Higher Education Institutions in Shanxi (STIP; grants 2016-92 and 2016-93), the Research Project of Shanxi Province Health and Family Planning Commission (grants 201301073, 2014028, 201601037, and 201601038), the Excellent talent science and technology innovation project of Shanxi Province (grants 201605D211029 and 201705D211018), Innovation Fund for Graduate Student of Shanxi Province (grants 2016-119 and 2016-101), Outstanding Youth Development Foundation of The First Hospital Affiliated with Shanxi Medical University (grant YR1601), Youth Foundation of The First Hospital Affiliated with Shanxi Medical University (grant YQ1503), Startup Foundation for Doctors of Shanxi Medical University (grant BS03201624), Startup Foundation for Doctors of Liaoning Province (grant 201601355), and Dalian medical science research project (grant 1711030).

REFERENCES

1. Cancer Genome Atlas Network (2015). Comprehensive genomic characterization of head and neck squamous cell carcinomas. Nature *517*, 576–582.
2. Gao, W., Zhang, C., Feng, Y., Chen, G., Wen, S., Huangfu, H., and Wang, B. (2012). Fascin-1, ezrin and paxillin contribute to the malignant progression and are predictors of clinical prognosis in laryngeal squamous cell carcinoma. PLoS ONE *7*, e50710.
3. Liu, H.C., Chen, G.G., Vlantis, A.C., Tong, M.C., and van Hasselt, C.A. (2008). Chemotherapy for laryngeal cancer—an apoptotic approach. Curr. Drug Targets *9*, 878–886.
4. Jenckel, F., and Knecht, R. (2013). State of the art in the treatment of laryngeal cancer. Anticancer Res. *33*, 4701–4710.
5. Lin, C., Zhang, S., Wang, Y., Wang, Y., Nice, E., Guo, C., Zhang, E., Yu, L., Li, M., Liu, C., et al. (2018). Functional role of a novel long noncoding RNA *TTN-AS1* in esophageal squamous cell carcinoma progression and metastasis. Clin. Cancer Res. *24*, 486–498.
6. Zhang, Y., Lu, Y., Zhang, C., Huang, D., Wu, W., Zhang, Y., Shen, J., Cai, Y., Chen, W., and Yao, W. (2018). FSCN-1 increases doxorubicin resistance in hepatocellular carcinoma through promotion of epithelial-mesenchymal transition. Int. J. Oncol. Published online March 20, 2018. https://doi.org/10.3892/ijo.2018.4327.
7. Wang, C.Q., Li, Y., Huang, B.F., Zhao, Y.M., Yuan, H., Guo, D., Su, C.M., Hu, G.N., Wang, Q., Long, T., et al. (2017). EGFR conjunct FSCN1 as a novel therapeutic strategy in triple-negative breast cancer. Sci. Rep. *7*, 15654.
8. Kozomara, A., and Griffiths-Jones, S. (2014). miRBase: annotating high confidence microRNAs using deep sequencing data. Nucleic Acids Res. *42*, D68–D73.
9. Zhao, X.D., Zhang, W., Liang, H.J., and Ji, W.Y. (2013). Overexpression of miR -155 promotes proliferation and invasion of human laryngeal squamous cell carcinoma via targeting SOCS1 and STAT3. PLoS ONE *8*, e56395.
10. Tian, Y., Fu, S., Qiu, G.B., Xu, Z.M., Liu, N., Zhang, X.W., Chen, S., Wang, Y., Sun, K.L., and Fu, W.N. (2014). MicroRNA-27a promotes proliferation and suppresses apoptosis by targeting PLK2 in laryngeal carcinoma. BMC Cancer *14*, 678.
11. Wang, F., Song, G., Liu, M., Li, X., and Tang, H. (2011). miRNA-1 targets fibronectin1 and suppresses the migration and invasion of the HEp2 laryngeal squamous carcinoma cell line. FEBS Lett. *585*, 3263–3269.
12. Uhlen, M., Zhang, C., Lee, S., Sjöstedt, E., Fagerberg, L., Bidkhori, G., Benfeitas, R., Arif, M., Liu, Z., Edfors, F., et al. (2017). A pathology atlas of the human cancer transcriptome. Science *357*, eaan2507.
13. Gao, W., Zhang, C., Ma, T., Wen, S., Fu, R., Zhao, D., Wu, Y., and Wang, B. (2016). Potential biomarkers and their regulatory relationships in laryngeal squamous cell carcinoma with lymph node metastasis revealed by integrating mRNA, microRNA and long non-coding RNA profiles. Int. J. Clin. Exp. Pathol. *9*, 5103–5116.
14. Zhang, C., Gao, W., Wen, S., Wu, Y., Fu, R., Zhao, D., Chen, X., and Wang, B. (2016). Potential key molecular correlations in laryngeal squamous cell carcinoma revealed by integrated analysis of mRNA, miRNA and lncRNA microarray profiles. Neoplasma *63*, 888–900.
15. Dweep, H., and Gretz, N. (2015). miRWalk2.0: a comprehensive atlas of microRNA-target interactions. Nat. Methods *12*, 697.
16. Pang, B., Wu, N., Guan, R., Pang, L., Li, X., Li, S., Tang, L., Guo, Y., Chen, J., Sun, D., et al. (2017). Overexpression of RCC2 enhances cell motility and promotes tumor metastasis in lung adenocarcinoma by inducing epithelial-mesenchymal transition. Clin. Cancer Res. *23*, 5598–5610.
17. Ma, Y., and Machesky, L.M. (2015). Fascin1 in carcinomas: its regulation and prognostic value. Int. J. Cancer *137*, 2534–2544.
18. El-Balat, A., Arsenic, R., Sänger, N., Karn, T., Becker, S., Holtrich, U., and Engels, K. (2016). Fascin-1 expression as stratification marker in borderline epithelial tumours of the ovary. J. Clin. Pathol. *69*, 142–148.
19. Karatas, O.F., Suer, I., Yuceturk, B., Yilmaz, M., Hajiyev, Y., Creighton, C.J., Ittmann, M., and Ozen, M. (2016). The role of miR-145 in stem cell characteristics of human laryngeal squamous cell carcinoma Hep-2 cells. Tumour Biol. *37*, 4183–4192.
20. Lei, C., Du, F., Sun, L., Li, T., Li, T., Min, Y., Nie, A., Wang, X., Geng, L., Lu, Y., et al. (2017). miR-143 and miR-145 inhibit gastric cancer cell migration and metastasis by suppressing MYO6. Cell Death Dis. *8*, e3101.
21. Larne, O., Hagman, Z., Lilja, H., Bjartell, A., Edsjö, A., and Ceder, Y. (2015). miR-145 suppress the androgen receptor in prostate cancer cells and correlates to prostate cancer prognosis. Carcinogenesis *36*, 858–866.
22. Cioce, M., Ganci, F., Canu, V., Sacconi, A., Mori, F., Canino, C., Korita, E., Casini, B., Alessandrini, G., Cambria, A., et al. (2014). Protumorigenic effects of mir-145 loss in malignant pleural mesothelioma. Oncogene *33*, 5319–5331.
23. Xing, A.Y., Wang, Y.W., Su, Z.X., Shi, D.B., Wang, B., and Gao, P. (2015). Catenin-δ1, negatively regulated by miR-145, promotes tumour aggressiveness in gastric cancer. J. Pathol. *236*, 53–64.
24. Mataki, H., Seki, N., Mizuno, K., Nohata, N., Kamikawaji, K., Kumamoto, T., Koshizuka, K., Goto, Y., and Inoue, H. (2016). Dual-strand tumor-suppressor microRNA-145 (miR-145-5p and miR-145-3p) coordinately targeted MTDH in lung squamous cell carcinoma. Oncotarget *7*, 72084–72098.
25. Feng, Y., Zhu, J., Ou, C., Deng, Z., Chen, M., Huang, W., and Li, L. (2014). MicroRNA-145 inhibits tumour growth and metastasis in colorectal cancer by targeting fascin-1. Br. J. Cancer *110*, 2300–2309.
26. Xu, W., Chang, J., Du, X., and Hou, J. (2017). Long non-coding RNA PCAT-1 contributes to tumorigenesis by regulating FSCN1 via miR-145-5p in prostate cancer. Biomed. Pharmacother. *95*, 1112–1118.
27. He, M., Zhan, M., Chen, W., Xu, S., Long, M., Shen, H., Shi, Y., Liu, Q., Mohan, M., and Wang, J. (2017). MiR-143-5p deficiency triggers EMT and metastasis by targeting HIF-1α in gallbladder cancer. Cell. Physiol. Biochem. *42*, 2078–2092.
28. Shi, H., Shen, H., Xu, J., Zhao, S., Yao, S., and Jiang, N. (2018). MiR-143-3p suppresses the progression of ovarian cancer. Am. J. Transl. Res. *10*, 866–874.
29. He, Z., Yi, J., Liu, X., Chen, J., Han, S., Jin, L., Chen, L., and Song, H. (2016). MiR-143-3p functions as a tumor suppressor by regulating cell proliferation, invasion and epithelial-mesenchymal transition by targeting QKI-5 in esophageal squamous cell carcinoma. Mol. Cancer *15*, 51.
30. Yamada, Y., Koshizuka, K., Hanazawa, T., Kikkawa, N., Okato, A., Idichi, T., Arai, T., Sugawara, S., Katada, K., Okamoto, Y., and Seki, N. (2018). Passenger strand of miR-145-3p acts as a tumor-suppressor by targeting MYO1B in head and neck squamous cell carcinoma. Int. J. Oncol. *52*, 166–178.
31. Iio, A., Takagi, T., Miki, K., Naoe, T., Nakayama, A., and Akao, Y. (2013). DDX6 post-transcriptionally down-regulates miR-143/145 expression through host gene NCR143/145 in cancer cells. Biochim. Biophys. Acta *1829*, 1102–1110.
32. Cui, R., Meng, W., Sun, H.L., Kim, T., Ye, Z., Fassan, M., Jeon, Y.J., Li, B., Vicentini, C., Peng, Y., et al. (2015). MicroRNA-224 promotes tumor progression in nonsmall cell lung cancer. Proc. Natl. Acad. Sci. USA *112*, E4288–E4297.
33. Alblazi, K.M., and Siar, C.H. (2015). Cellular protrusions—lamellipodia, filopodia, invadopodia and podosomes—and their roles in progression of orofacial tumours: current understanding. Asian Pac. J. Cancer Prev. *16*, 2187–2191.

34. Gimona, M., Buccione, R., Courtneidge, S.A., and Linder, S. (2008). Assembly and biological role of podosomes and invadopodia. Curr. Opin. Cell Biol. *20*, 235–241.

35. Condeelis, J., and Segall, J.E. (2003). Intravital imaging of cell movement in tumours. Nat. Rev. Cancer *3*, 921–930.

36. Johnson, H.E., King, S.J., Asokan, S.B., Rotty, J.D., Bear, J.E., and Haugh, J.M. (2015). F-actin bundles direct the initiation and orientation of lamellipodia through adhesion-based signaling. J. Cell Biol. *208*, 443–455.

37. Jayo, A., Malboubi, M., Antoku, S., Chang, W., Ortiz-Zapater, E., Groen, C., Pfisterer, K., Tootle, T., Charras, G., Gundersen, G.G., and Parsons, M. (2016). Fascin regulates nuclear movement and deformation in migrating cells. Dev. Cell *38*, 371–383.

38. Winkelman, J.D., Suarez, C., Hocky, G.M., Harker, A.J., Morganthaler, A.N., Christensen, J.R., Voth, G.A., Bartles, J.R., and Kovar, D.R. (2016). Fascin- and α-actinin-bundled networks contain intrinsic structural features that drive protein sorting. Curr. Biol. *26*, 2697–2706.

39. Gonzalez, D.M., and Medici, D. (2014). Signaling mechanisms of the epithelial-mesenchymal transition. Sci. Signal. *7*, re8.

40. Izdebska, M., Zielińska, W., Grzanka, D., and Gagat, M. (2018). The role of actin dynamics and actin-binding proteins expression in epithelial-to-mesenchymal transition and its association with cancer progression and evaluation of possible therapeutic targets. BioMed Res. Int. *2018*, 4578373.

41. Peng, J.M., Bera, R., Chiou, C.Y., Yu, M.C., Chen, T.C., Chen, C.W., Wang, T.R., Chiang, W.L., Chai, S.P., Wei, Y., et al. (2018). Actin cytoskeleton remodeling drives epithelial-mesenchymal transition for hepatoma invasion and metastasis in mice. Hepatology *67*, 2226–2243.

42. Wang, H., Tao, L., Jin, F., Gu, H., Dai, X., Ni, T., Feng, J., Ding, Y., Xiao, W., Qian, Y., and Liu, Y. (2017). Cofilin 1 induces the epithelial-mesenchymal transition of gastric cancer cells by promoting cytoskeletal rearrangement. Oncotarget *8*, 39131–39142.

43. Kent, O.A., McCall, M.N., Cornish, T.C., and Halushka, M.K. (2014). Lessons from miR-143/145: the importance of cell-type localization of miRNAs. Nucleic Acids Res. *42*, 7528–7538.

44. Xia, W., Chen, Q., Wang, J., Mao, Q., Dong, G., Shi, R., Zheng, Y., Xu, L., and Jiang, F. (2015). DNA methylation mediated silencing of microRNA-145 is a potential prognostic marker in patients with lung adenocarcinoma. Sci. Rep. *5*, 16901.

45. Zaman, M.S., Chen, Y., Deng, G., Shahryari, V., Suh, S.O., Saini, S., Majid, S., Liu, J., Khatri, G., Tanaka, Y., and Dahiya, R. (2010). The functional significance of microRNA-145 in prostate cancer. Br. J. Cancer *103*, 256–264.

46. Ehrich, M., Nelson, M.R., Stanssens, P., Zabeau, M., Liloglou, T., Xinarianos, G., Cantor, C.R., Field, J.K., and van den Boom, D. (2005). Quantitative high-throughput analysis of DNA methylation patterns by base-specific cleavage and mass spectrometry. Proc. Natl. Acad. Sci. USA *102*, 15785–15790.

YMTHE, Volume *27*

Supplemental Information

Promoter Methylation-Regulated miR-145-5p Inhibits Laryngeal Squamous Cell Carcinoma Progression by Targeting *FSCN1*

Wei Gao, Chunming Zhang, Wenqi Li, Huizheng Li, Jiangwei Sang, Qinli Zhao, Yunfeng Bo, Hongjie Luo, Xiwang Zheng, Yan Lu, Yong Shi, Dongli Yang, Ruiping Zhang, Zhenyu Li, Jiajia Cui, Yuliang Zhang, Min Niu, Jun Li, Zhongqiang Wu, Huina Guo, Caixia Xiang, Juan Wang, Juan Hou, Lu Zhang, Rick F. Thorne, Yongping Cui, Yongyan Wu, Shuxin Wen, and Binquan Wang

Figure S1

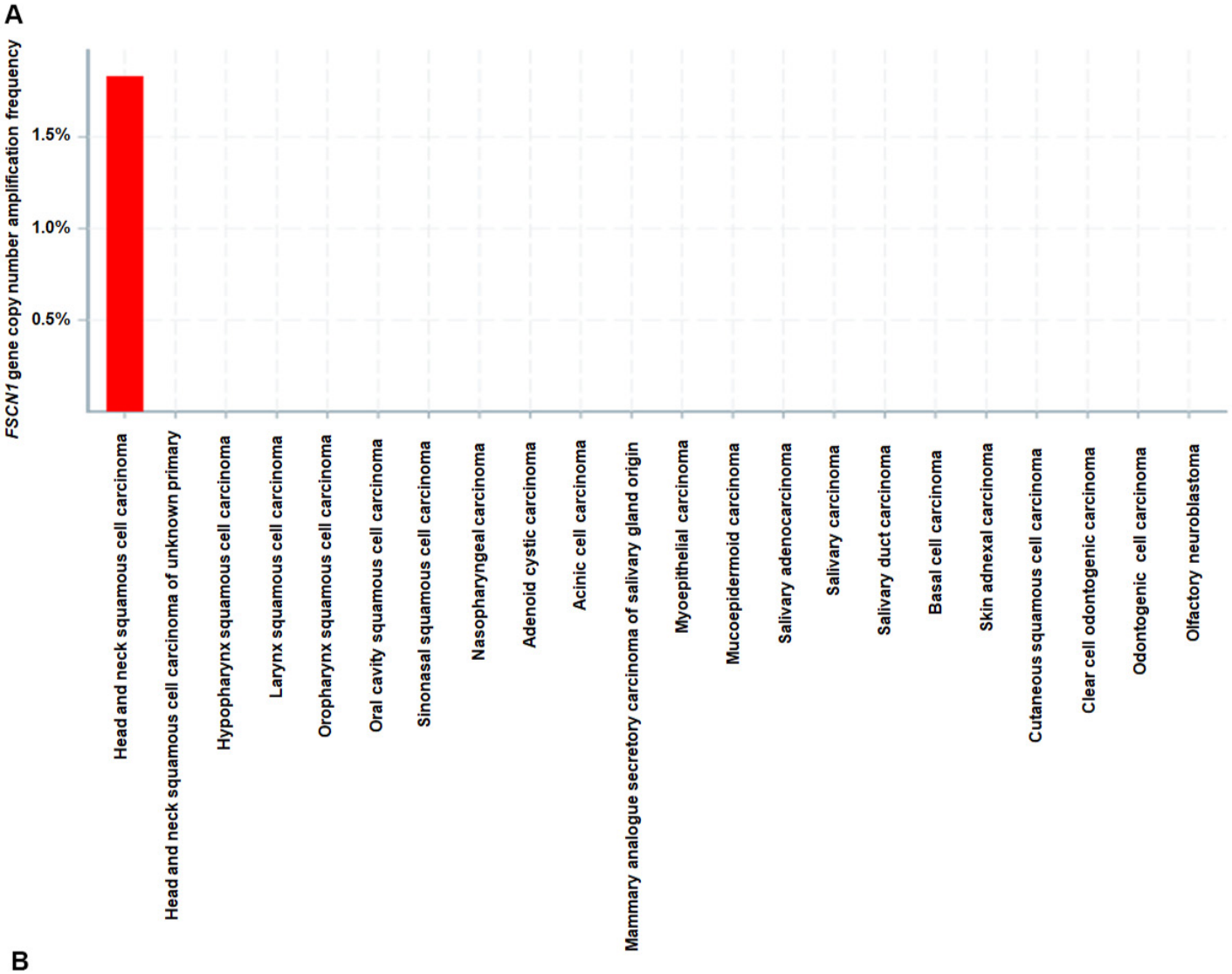
A
FSCN1 gene copy number amplification frequency
1.5%
1.0%
0.5%
Head and neck squamous cell carcinoma
Head and neck squamous cell carcinoma of unknown primary
Hypopharynx squamous cell carcinoma
Larynx squamous cell carcinoma
Oropharynx squamous cell carcinoma
Oral cavity squamous cell carcinoma
Sinonasal squamous cell carcinoma
Nasopharyngeal carcinoma
Adenoid cystic carcinoma
Acinic cell carcinoma
Mammary analogue secretory carcinoma of salivary gland origin
Myoepithelial carcinoma
Mucoepidermoid carcinoma
Salivary adenocarcinoma
Salivary carcinoma
Salivary duct carcinoma
Basal cell carcinoma
Skin adnexal carcinoma
Cutaneous squamous cell carcinoma
Clear cell odontogenic carcinoma
Odontogenic cell carcinoma
Olfactory neuroblastoma

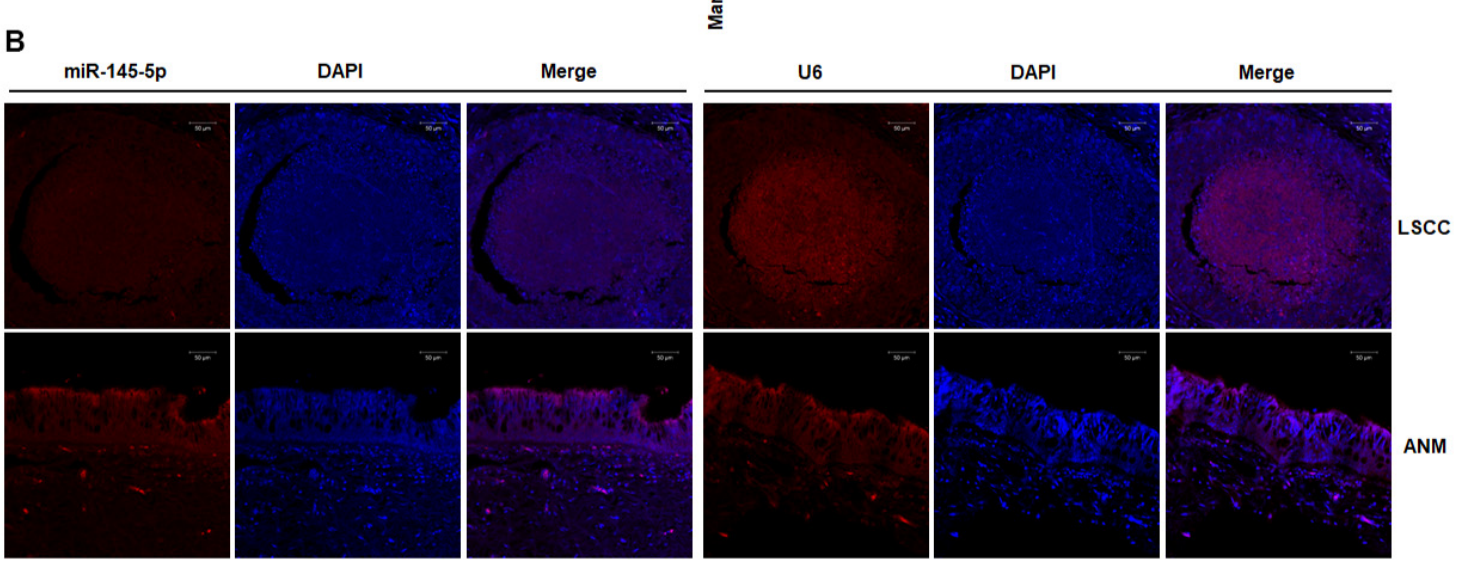
B
miR-145-5p
DAPI
Merge
U6
DAPI
Merge
LSCC
ANM

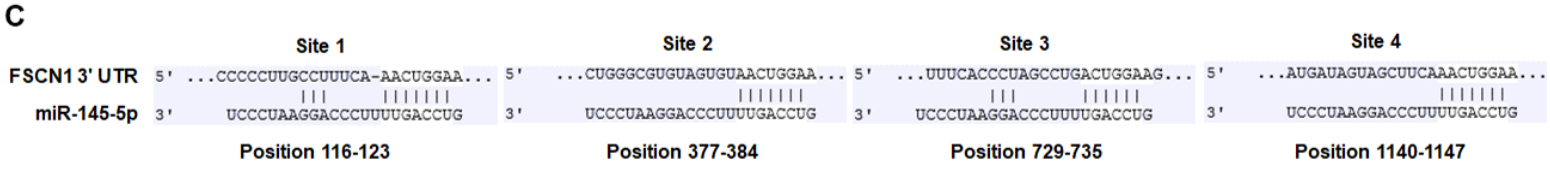
C
Site 1
Site 2
Site 3
Site 4
FSCN1 3' UTR
miR-145-5p
Position 116-123
Position 377-384
Position 729-735
Position 1140-1147

Figure S2

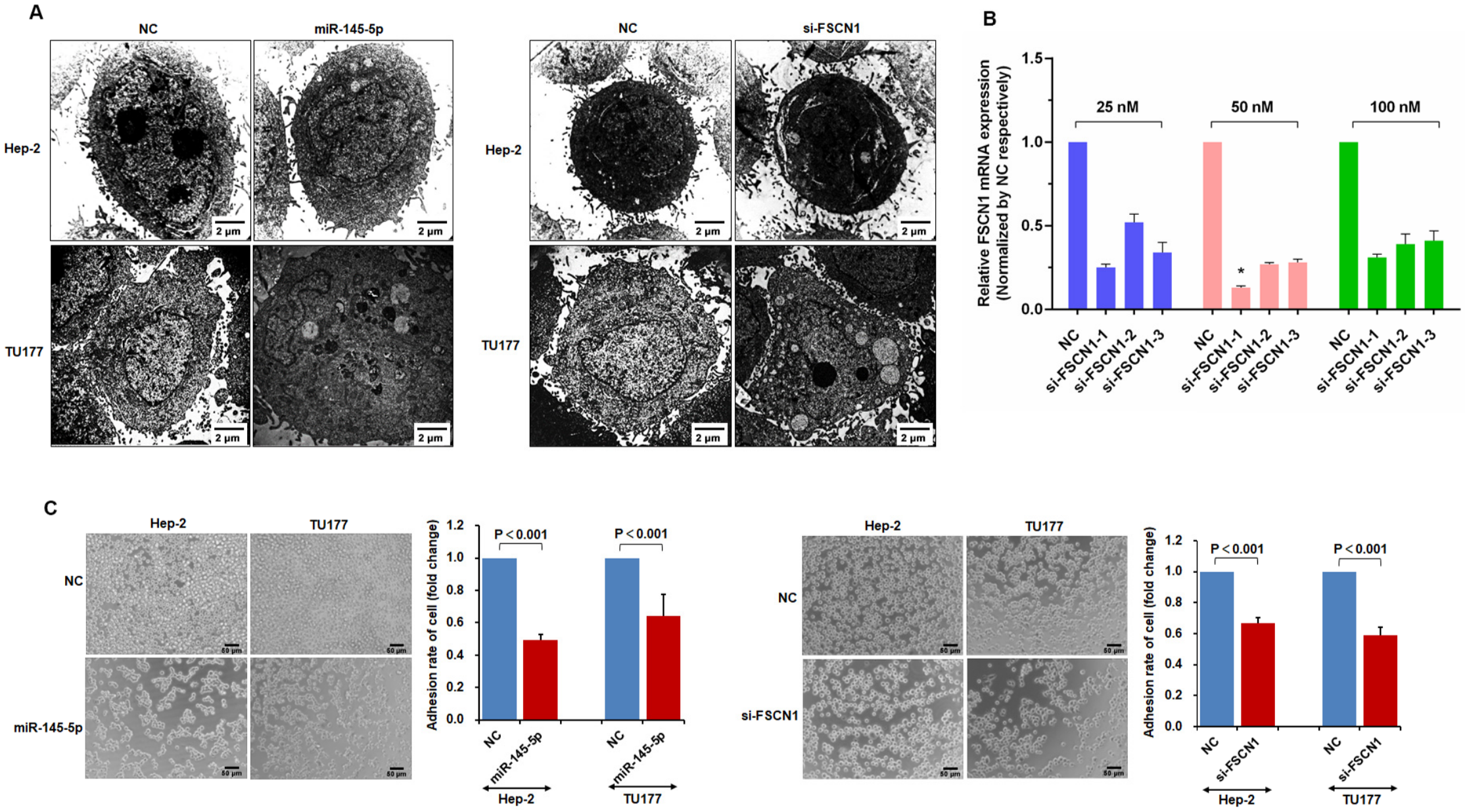
A
NC
miR-145-5p
si-FSCN1
Hep-2
TU177
2 μm
B
Relative FSCN1 mRNA expression
(Normalized by NC respectively)
25 nM
50 nM
100 nM
NC
si-FSCN1-1
si-FSCN1-2
si-FSCN1-3
C
Adhesion rate of cell (fold change)
P < 0.001
50 μm

Figure S3

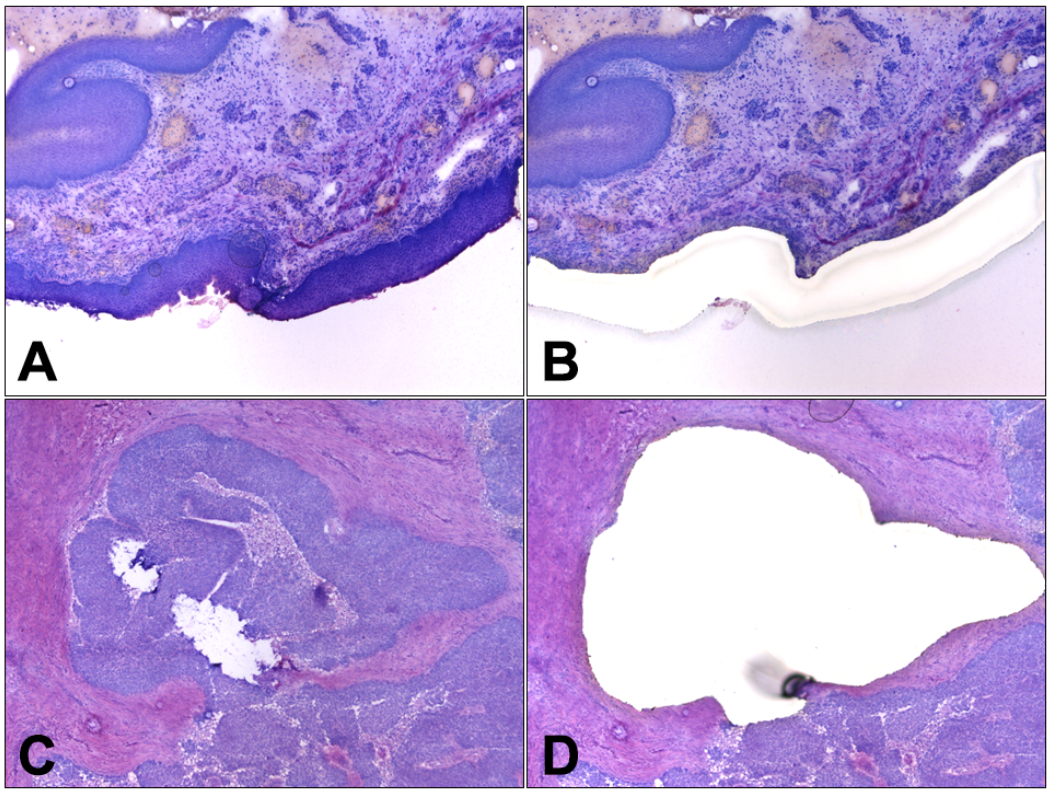

Figure S4

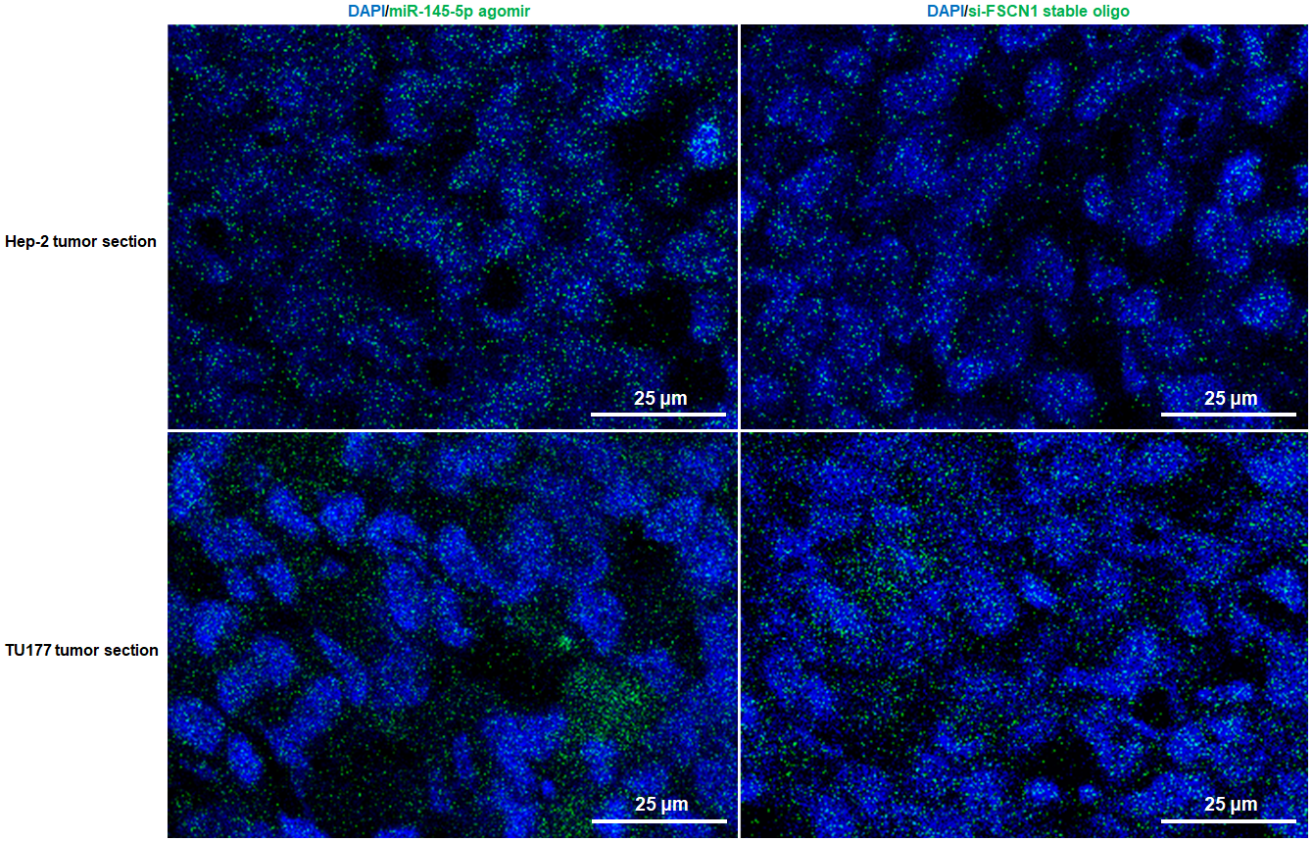
DAPI/miR-145-5p agomir
DAPI/si-FSCN1 stable oligo
Hep-2 tumor section
TU177 tumor section
25 μm
25 μm
25 μm
25 μm

Supplemental legends

Figure S1. **(A)** Copy number variation analysis of *FSCN1* gene in 1685 head and neck cancer samples (including LSCC) from TCGA dataset performed with cBioPortal v1.13.1 (http://www.cbioportal.org/index.do). **(B)** Fluorescence *in situ* hybridization of miR-145-5p in LSCC and ANM tissue. Expression of U6 RNA was an internal control. **(C)** Complementary binding sites of miR-145-5p on 3'-UTR of FSCN1.

Figure S2. (A) Hep-2 and TU177 cells were transfected with miR-145-5p mimic or siRNA oligos targeting FSCN1 for 48 h; apoptotic bodies were observed by TEM. **(B)** Screening of FSCN1 siRNA. qPCR analysis of mRNA level of FSCN1 in Hep-2 cells transfected with siRNAs targeting 3 different sequences of FSCN1 mRNA at the indicated concentrations for 48 h. **(C)** Hep-2 and TU177 cells were transfected with miR-145-5p mimic or siRNA oligos targeting FSCN1 for 48 h; cell adhesive ability was measured. Data are mean ± SD of three independent experiments.

Figure S3. Laser capture microdissection (LCM) of LSCC or paired ANM fresh frozen tissues. Representative images of ANM tissue section before **(A)** and after **(B)** laser capture microdissection (LCM). Representative images of LSCC fresh tissue sections before **(C)** and after **(D)** LCM.

Figure S4. Verification of delivery efficiency of RNA oligos injected into xenograft tumors**.** Hep-2 or TU177 cells were subcutaneously injected into the flanks of BALB/C nude mice to generate xenograft tumors. When the tumors had grown to 0.5 mm3, FAM labeled miR-145-5p agomir or FSCN1 siRNA stable oligos were subcutaneously injected into the tumor site as follows: multi-point injection with 0.1 ml oligos (10 nmol), 2 times/week/position and on the first and fourth day per week. Tumors were separated 96 h after injection, then frozen sections were prepared and observed under confocal laser scanning microscopy. Representative images show distribution and level of miR-145-5p agomir or FSCN1 siRNA in tumors. The nuclei were stained with DAPI (blue). The miR-145-5p agomir or FSCN1 siRNA can be seen as green fluorescent dots.

Supplemental Table S1. Prediction of miRNA targeting FSCN1. Potential miRNA of FSCN1 was predicted with miRwalk-2, the information of potential binding site was shown in the Excel file.

Supplemental Table S2. Differentially expressed miRNAs from microarray data of paired LSCC and adjacent normal margin tissues.

Gene Name	P value	Fold Change	Style
hsa-miR-486-5p	0.04	8.2	Down
hsa-miR-204-5p	<0.001	5.02	Down
hsa-miR-139-5p	0.03	3.2	Down
hsa-miR-145-5p	0.02	2.74	Down
hsa-miR-1305	0.02	2.4	Down
hsa-miR-1225-3p	0.03	2.1	Down
hsa-miR-21-5p	0	8.14	Up
hsa-miR-21-3p	0	5.76	Up
hsa-miR-135b-5p	0.02	5.72	Up
hsa-miR-210	0.02	5.66	Up
hsa-miR-130b-3p	<0.001	5.17	Up
hsa-miR-7-5p	0.02	4.62	Up
hsa-miR-222-3p	0.04	3.56	Up
hsa-miR-19a-3p	0.01	3.55	Up
hsa-miR-181b-5p	0.01	3.35	Up
hsa-miR-106b-5p	0.01	3.3	Up
hsa-miR-185-5p	0.03	3.03	Up
hsa-miR-19b-3p	0.02	3.01	Up
hsa-miR-151-3p	0.03	2.98	Up
hsa-miR-362-5p	0.02	2.72	Up
hsa-miR-93-5p	<0.001	2.61	Up
hsa-miR-20a-5p	0.01	2.56	Up
hsa-miR-425-5p	0.01	2.52	Up
hsa-miR-20b-5p	0.02	2.38	Up
hsa-miR-374b-5p	0.04	2.36	Up
hsa-miR-181a-5p	<0.001	2.29	Up
hsa-miR-27a-3p	0.03	2.28	Up
hsa-miR-424-5p	0.04	2.26	Up
hsa-miR-152	0.01	2.18	Up

Supplemental Table S3. Clinical features of 188 LSCC patients.

Parameters	Number of Cases（%）
Age	
≤60	89（47.3）
＞60	99（52.7）
Sex	
Female	21（11.2）
Male	167（88.8）
Primary cancer site	
Glottic	101（53.7）
Supraglottic	83（44.1）
Subglottic	4（2.1）
Differentiation	
High	72（38.3）
Medium	75（39.9）
Low	41（21.8）
T staging[1]	
T1	53（28.2）
T2	58（30.9）
T3	41（21.8）
T4	36（19.1）
Cervical lymph node metastasis	
N0	142（75.5）
N+	46（24.5）
Distant metastasis	
M0	183（97.3）
M1	5（2.7）
Clinical stage	
I	51（27.1）
II	45（23.9）
III	47（25.0）
IV	45（23.9）
Smoke preoperatively[2]	
No	75（39.9）
Yes	113（60.1）

[1]TNM Staging is referring to the 7th UICC TNM Staging Criteria

[2]Smoker is referring to definition from WHO 1997: at least one cigarette each day continuous or accumulation for six months.

Supplemental Table S4. COX regression analysis of miR-145-5p/FSCN1 expression combination

Prognostic Factor	Regression Coefficient	Standard Error	Wald	*P* value	Relative Risk（*RR*）	*95.0% CI*
miR145(High)/FSCN1(Low)					1.00	
miR145(Low)/FSCN1(Low)	0.260	1.23	0.05	0.833	1.30	0.12～14.42
miR145(High)/FSCN1(High)	2.70	0.79	11.67	***0.001***	14.85	3.16～69.85
miR145(Low)/FSCN1(High)	2.54	0.77	11.01	***0.001***	12.69	2.83～56.91

Supplemental Table S5. COX regression analysis of FSCN1 protein expression.

Prognostic Factor	Regression Coefficient	Standard Error	Wald	*P* value	Relative Risk (RR)	*95.0% CI*
Age（>60）	0.87	0.30	8.518	***0.001***	2.39	1.33～4.29
Neck lymph node metastasis	1.096	0.28	15.28	***<0.001***	2.99	1.73～5.19
Distant metastasis	2.245	0.52	18.85	***0.002***	9.44	3.43～26.01
Smoke preoperatively	0.97	0.35	7.55	***0.016***	2.65	1.32～5.30
FSCN1 high-expressed	2.507	0.64	15.26	***0.001***	12.27	3.49～43.19

Supplemental Table S6. Clinical features of LSCC samples underwent DNA methylation analysis.

Parameters	Number of Cases
Age	
≤60	5
＞60	7
Sex	
Female	1
Male	11
Primary cancer site	
Glottic	2
Supraglottic	8
Transglottic	2
Differentiation	
High	5
Medium	4
Low	3
T staging[1]	
T1	4
T2	1
T3	4
T4	3
Cervical lymph node metastasis	
N0	9
N+	3
Distant metastasis	
M0	12
M1	0
Clinical stage	
I	3
II	1
III	4
IV	4
Smoke preoperatively[2]	
No	0
Yes	12

[1]TNM Staging is referring to the 7th UICC TNM Staging Criteria
[2]Smoker is referring to definition from WHO 1997: at least one cigarette each day continuous or accumulation for six months.

RNA extraction and qPCR analysis

Total RNA was extracted from frozen cancer tissues by use of TRIzol reagent (Invitrogen). For formalin-fixed paraffin-embedded (FFPE) samples, total RNA was extracted by using the RecoverAll Total Nucleic Acid Isolation Kit for FFPE (Ambion). cDNA was synthesized from total RNA by using the PrimeScript RT Kit (TaKaRa, Dalian, China). qPCR was performed on the ABI 7500 FAST real-time PCR system (Applied Biosystems, Foster City, CA, USA). The procedures for qPCR were 95°C for 30 sec, followed by 40 cycles of 95°C for 10 sec and 60°C for 30 sec. The $2^{-\Delta\Delta ct}$ method was used to calculate the relative expression level of target genes. U6 RNA and 18S rRNA were served as internal control for miR-145-5p and FSCN1, respectively. The primer sequences used were for Hsa-miR-145 F: ACACTCCAGCTGGGGTCCAGTTTTCCCAGGAA;
Hsa-miR-145 R: CTCAACTGGTGTCGTGGA;
U6-F: CTCGCTTCGGCAGCACA;
U6-R: AACGCTTCACGAATTTGCGT;
FSCN1-F: AGCTGCTACTTTGACATCGA;
FSCN1-R: TCATGAGGAAGAGCTCTGAGT;
18S RNA-F: CCTGGATACCGCAGCTAGGA;
18S RNA-R: GCGGCGCAATACGAATGCCCC.

Antibodies

FSCN1 (Cat#ab126772) and Cyclin D1 (Cat#ab16663) rabbit monoclonal antibodies were purchased from Abcam (Cambridge, MA); GAPDH mouse monoclonal antibody (Cat#HC301) was purchased from TransGen Biotech. (Beijing, China); Cleaved Caspase-3 (Cat#9664S), E-cadherin (Cat#3195S), N-cadherin (Cat#13116S), Vimentin (Cat#5741S), and Snail (Cat#3879S) rabbit monoclonal antibodies were purchased from Cell Signaling Technology, Inc. (Danvers, MA); MMP-2 (Cat#sc-13594) and MMP-9 (Cat#sc-21733) mouse monoclonal antibodies were purchased from Santa Cruz Biotechnology, Inc. (Dallas, TX).

Western blot analysis

Tissue protein lysates were prepared by use of the Tissue Protein Extraction Reagent and Proteasome Inhibition Mixture (Cwbiotech, Beijing) according to the manufacturer's instructions. Cell protein lysates were prepared by using RIPA buffer (Pierce). Protein concentration was determined by using a BCA kit (Cwbiotech). Protein with 2× SDS loading buffer was boiled for 10 min, underwent SDS-PAGE and was transferred to PVDF membranes (Millipore), which were blocked with 5% nonfat milk, then incubated with primary antibody at 4 °C overnight, then horseradish peroxidase-conjugated secondary antibody for 1 h at room temperature. Blots were developed with ECL substrate (Millipore).

Generation of reporter constructs

The wild-type FSCN1-3' UTR reporter construct was constructed by amplifying and inserting the 3' UTR of FSCN1 into the psiCHECK-2 vector. Mutated FSCN1-3' UTR sequences were obtained by overlap extension PCR, and resulting fragments were inserted into psiCHECK-2 to generate mutated reporter constructs. All constructs were verified by DNA sequencing.

Luciferase reporter assay

Luciferase assay involved use of the Dual-Luciferase Reporter Assay System (Promega, Madison, WI) following the manufacturer's instructions. Briefly, after 48-h transfection, growth media was removed and cells were washed gently with PBS twice, then 100 μl/well passive lysis buffer was added with gentle rocking for 15 min at room temperature. Cell lysates were collected for luciferase assay.

Immunohistochemistry staining and analysis

Paraffin sections were dewaxed and re-hydrated in ethanol in descending concentrations (100%, 90%, 80%, 70%). For antigen retrieval, samples were processed in an autoclave for 2 min, 15 sec with sodium citrate (pH 6). Endogenous peroxidase activity was blocked by immersing tissue sections in 3% H2O2 in methanol (v/v) at room temperature for 10 min, then washing with PBS. Nonspecific background staining was reduced by incubating sections with nonimmune goat serum (Boster Co., Wuhan, China) for 15 min at room temperature. Sections were incubated with antibody for FSCN1 (1:200, Vector Laboratories) overnight in a moist chamber at 4 °C and washed 3 times with PBST for 5 min. Sections were incubated with the secondary antibody from the Max Vision HRP-Polymer anti-Mouse IHC kit (MaxinBio, Fuzhou, China) for 15 min at room temperature, then washed 3 times for 5 min with PBST. The DAB substrate detection system was used (Vector Laboratories). Counterstaining was with hematoxylin, then sections were dehydrated and mounted with coverslips. Two independent pathologists, blinded to the clinical parameters, calculated the immunoreactivity score for FSCN1 expression. Immunohistochemical staining was assessed semiquantitatively by the proportion of tumor cells with positive staining and staining intensity. Staining intensity was scored as 0 (no staining), 1 (weak intensity), 2 (moderate intensity) and 3 (strong intensity). Percentage of positive staining tumor cells in tumor tissue was for score 1, ≤ 10%; 2, 11–50%; 3, 51–80%; and 4, 81-100%. The final assessment was calculated as mean combined score for staining intensity and positive-stained cell percentage, ranging from 1 to 7. Specimens were divided into 3 groups of expression by overall scores: negative (1), low expression (2-5), and high expression (6-7). Negative and low-expression specimens were defined as low expression in statistical analysis.

Cell proliferation assay

Cell proliferation was determined by using the Cell Counting Kit-8 (DOJINDO, Beijing). Moreover, the percentage of cells incorporating EdU was evaluated by using the Cell-Light EdU imaging kit (RiboBio Co., Guangzhou, China).

Cell adhesion assay

Hep-2 and TU177 cells transfected with miR-145-5p mimic or si-FSCN1 were plated in 96-well plates, then cell adhesion was measured by using the Cell Counting Kit-8 (DOJINDO). The absorbance was measured by using a microplate reader Multiscan MK3 (ThermoFisher Scientific), and background absorbance was corrected by using the CCK-8 solution without cells.

Apoptosis analysis

Apoptosis analysis of Hep-2 and TU177 cells involved use of the Annexin V Apoptosis Detection Kit I (BD, NJ, USA), and apoptosis was analyzed by FACSCalibur flow cytometry (BD, San Jose, CA, USA). Apoptotic cells in LSCC tumor tissues were detected by using the DeadEnd™ Colorimetric TUNEL System (Promega) following the manufacturer's instructions.

Cell cycle analysis

An amount of 1×10^6 cells was harvested 48 h after transfection and fixed overnight in 70% ice-cold ethanol and 4 ℃. Cells were stained with 50 μg/ml propidium iodide (PI), 100 U/ml RNase A, and 0.2% Triton X-100 for 30 min, then quantified by FACSCalibur flow cytometry (BD), and data were analyzed by using ModFit software.

Transwell migration assay

After transfection, 1×10^6 cells were plated in 100 μl DMEM-F12 medium without serum, then incubated in Transwell plates at 37 °C and 5% CO2 for 24 h and 48 h; the upper side of the filter membrane was wiped with a cotton swab to remove the cell debris. Cells on the lower side of the insert

filter were stained with crystal violet for 10 min. The absorbance at OD570 was measured by using the microplate reader Multiscan MK3 (ThermoFisher Scientific).

Cell invasion assay

Matrigel was thawed at 4 °C, then 40 μl Matrigel solution (Matrigel : medium=1:3) was added to a precooled Transwell insert and solidified in a 37°C incubator for 2 h to form a thin gel layer. Cells were resuspended with serum-free medium at 1 x 10^5 cells/well. The upper side of the filter membrane was wiped with a cotton swab to remove cell debris, then cells on the lower side of the insert filter were stained with crystal violet for 10 min and washed with PBS once. The absorbance at OD570 was measured by using the microplate reader Multiscan MK3.

Microscopy imaging and staining

Images were captured by using the JSM-6360LV scanning electron microscope (JEOL, Tokyo). F-actin staining was performed using Rhodamine-Phalloidin (Cytoskeleton, Inc., Denver, CO.) according to the manufacturer's instructions. Briefly, fixed cells were incubated with 200 μl Rhodamine-Phalloidin (200 nM), counterstained with DAPI (Sigma) and imaged by using a confocal laser-scanning microscope (Leica TCS SP8).

Laser capture microdissection

Frozen sections of LSCC or paired ANM fresh tissue was stained with Histogene staining solution (Thermo Fisher Scientific, Waltham, MA) and dehydrated in ascensional concentrations ethanol (70%, 80%, 90%, 100%). Laser capture microdissection was performed on Leica LMD6500 laser microdissection Systems (Leica Microsystems CMS GmbH, Wetzlar, Germany).

Primer sequences for DNA methylation of miR-145 promoter

1. Primer sequence for Massarray methylation analysis of miR-145 promoter

F：AGGAAGAGAGAGAGAGGAAGTTGTTAAATTTAGGT-3'

R：CAGTAATACGACTCACTATAGGGAGAAGGCTAATTTAAAACATAATTCATAAACCCT

2. Primer sequences for pyrosequencing methylation analysis of miR-145 promoter

Amplified fragments	Primer name	Nucleotide sequence
Fragment 1	miR-145-F1	TTTGGTAGGAGATTGGGGAATAT
	miR-145-R1	Biotin-CTCTTCTACATCCAACCCCATCTA
	Sequencing Primer 1	AGTTTTGGGGGTGGG
Fragment 2	miR-145-F2	TTTGGTAGGAGATTGGGGAATAT
	miR-145-R2	Biotin-CTCTTCTACATCCAACCCCATCTA
	Sequencing Primer 2	TTATTTTTTTTGAGAGTAATAA
Fragment 3	miR-145-F3	GGGTTGGATGTAGAAGAGAATTT
	miR-145-R3	Biotin-TTTCCAAAAATCCCCATCTTAA
	Sequencing Primer 3	TTAGTTGGTTTTTAGGGATA